POLITECNICO DI TORINO
Repository ISTITUZIONALE

Measuring the particles in fly ash by means of an image segmentation

Original
Measuring the particles in fly ash by means of an image segmentation / Sparavigna, A.C.. - In: PHILICA. - ISSN 1751-3030. - ELETTRONICO. - 2017:1105(2017).

Availability:
This version is available at: 11583/2678735 since: 2017-08-30T19:07:06Z

Publisher:
Philica

Published
DOI:

Terms of use:

This article is made available under terms and conditions as specified in the corresponding bibliographic description in the repository

Publisher copyright

(Article begins on next page)

22 November 2026

electronics

MDPI

Review

Implantable Antenna–Biosensor Systems for Cancer Surveillance: Evidence, Biological Interfaces, and a Translational Design Framework

Sumer Singh Singhwal

Department of Electronics and Telecommunications, Politecnico di Torino, 10129 Turin, Italy; sumer.singhwal@polito.it

Abstract

An implanted antenna can support cancer surveillance when a disease-related change produces a reproducible measurement that can be distinguished from relevant benign changes and interpreted within a defined clinical pathway. This critical review connects cancer biomarkers, local physiological changes, biosensor mechanisms, and in-body RF interfaces across major tumour sites, with particular attention to oral, head and neck, and lung cancer. Three approaches are distinguished: antennas that sense tissue dielectric properties, chemically functionalized antenna immunosensors, and separate cancer sensors coupled to implanted radio telemetry. The unresolved problem is durable, site- and endpoint-specific surveillance under realistic sampling, inflammatory, biointerface, and wireless constraints. Comparative evidence tables identify measured specimens, demonstrated endpoints, candidate sensor–antenna combinations, and decisive missing experiments. A compact quantitative framework links target access, binding, RF observability, confounder control, read availability, and false-alert burden. A gated development workflow, illustrated using a published CEA antenna, converts these constraints into testable research requirements. The outcome is a research roadmap for clinically interpretable local warnings.

Keywords: implantable antenna; cancer recurrence; biosensor; tumour biomarker; wireless sensing; oral cancer; head and neck cancer; lung cancer; immunosensor; translational bioelectronics

1. Introduction

Implantable cancer surveillance requires a complete path from a disease-related change to a measurement that can support a clinical decision. The device must sample the relevant molecular target or tissue change, the measurement must distinguish it from relevant interferents, and the wireless readout must preserve that information over time. Antenna matching and gain describe the communication interface; biomarker association in collected plasma describes a different part of this pathway. A useful surveillance system must connect both through a defined biological compartment and a validated warning rule.

The clinical motivation is substantial. GLOBOCAN estimated approximately 20 million new cancer cases and 9.7 million deaths worldwide in 2022 [1]. Recurrence may follow persistence of local tumour cells, regional spread, or reactivation of disseminated disease. Contemporary work on cancer dormancy emphasizes that biologically important residual cells can remain quiescent before producing detectable progression [2]. Therefore, a local implant may detect a changing surgical bed while missing a distant lesion, and a physiolog-

Check for updates

Academic Editor: Sergey Shleev

Received: 19 October 2026
Revised: 12 November 2026
Accepted: 17 November 2026
Published: 19 November 2026

Copyright: © 2026 by the author. Licensee MDPI, Basel, Switzerland. This article is an open access article distributed under the terms and conditions of the Creative Commons Attribution (CC BY) license.

ical disturbance may appear only after the earliest molecular changes. These limitations define the intended observation window.

Relevant technological intersections already exist. Wang et al. proposed an implanted antenna responsive to breast-tissue dielectric changes [3]. Chen et al. functionalized an implanted antenna with an Au-decorated graphene immunosensing layer for carcinoembryonic antigen (CEA) [4]. Kim et al. and Nie et al. combined implanted optical measurements with wireless power and Bluetooth communication in cancer models [5,6]. Weng et al. reported a tumour-targeted optical implant with ultrasound power and Bluetooth telemetry for postoperative breast-cancer recurrence experiments [7]. These studies establish precedents for both cancer-associated antenna sensing and cancer biosensors with implanted RF communication.

The remaining translational gap is the lack of a broadly validated route from a clinically supported, site-specific target to a stable implanted RF warning system with demonstrated longitudinal specificity, read availability, and clinical value. Molecular recognition, local physiological sensing, and RF communication have progressed at different rates and under different experimental conditions. In oral, head and neck, and lung cancer, particularly, strong clinical biomarker studies have not automatically yielded chronically validated cancer-surveillance antenna systems.

The contribution here is a decision procedure for a specified surveillance indication, rather than a new antenna principle. The observed endpoint is compared with the event to be detected; biomarker access at the proposed implant and repeatable sensing through a selective wet interface are then assessed. Recovery of that signal at an external reader under realistic variation is required before a frozen longitudinal rule is evaluated against recurrence and available nonimplanted tests. The worked CEA example identifies measurements that could disqualify an apparently sensitive antenna before implantation; the oral and thoracic cases show why specimen access and event coverage change the preferred architecture.

Prior reviews provide important but different foundations (Table 1). The present synthesis does not claim novelty for miniaturization, passive coupling, microwave immunosensing, or the existence of cancer-monitoring implants. Its narrower contribution is to connect target–compartment evidence, serviceable recognition chemistry, the reader-level decision variable, and event-window clinical validity in one falsifiable workflow.

Table 1. Position relative to representative prior reviews. The last row states the added decision rather than claiming that its constituent mechanisms are new.

Review Focus	Established Contribution	Surveillance Decision Not Resolved There
Implantable antennas [8]	Tissue loading, size, band, link, and biocompatibility	Which cancer event is accessible at a specific interface?
Passive implant sensors [9]	Coupling, packaging, and passive readout options	Does the accessible analyte remain selective and repeatable during healing?
Insertable biosensors [10]	Longitudinal sensing materials and external interrogation	Is a cancer signal retained through a complete in-body reader and warning rule?
Microwave oncology sensing [11]	Resonator and dielectric approaches, including cancer biomarkers	Does an assay response transfer to a packaged, chronically interrogated implant?
Salivary cancer biomarkers [12]	Candidate oral targets and evidence limitations	Does the same target reach an exposed or buried oral sensor before a defined event?
This review	Target–compartment–interface–reader–warning evidence map	Advance, revise, or stop at five endpoint-specific validation decisions

2. Literature Identification and Evidence Appraisal

This is a critical narrative review, not a systematic search or a meta-analysis. Studies were identified through targeted searches of PubMed/MEDLINE, IEEE Xplore, and publisher platforms (Elsevier ScienceDirect, Springer Nature, Wiley, and MDPI); citation lists of the closest device and clinical studies were also followed. The principal coverage was January 2010–October 2026, with earlier seminal work retained for foundational clinical and sensor evidence, transport, recognition and detection theory, and early implant precedents. The last targeted literature check was on 3 November 2026; bibliographic metadata were rechecked on 3 November 2026. Representative combined queries were ("implantable antenna" OR "implantable sensor" OR "passive resonator") AND (cancer OR tumour OR recurrence), and (saliva OR interstitial OR lymphatic OR plasma) AND (biomarker OR ctDNA OR pH) AND (oral OR head and neck OR lung). Searches and reference selection were purposive: duplicate independent screening and PRISMA accounting were not performed, and the total number of eligible studies worldwide was not estimated.

Device studies were prioritized if they disclosed a sensing transducer, placement or test matrix, measured feature, and interrogation method and were retained when they clarified an important negative boundary. Clinical studies were selected for a defined cancer site, specimen, population, and surveillance or transformation endpoint. Routine antenna-only telemetry, external microwave imaging, and unverified tumour-detection claims were not counted as direct implant's cancer-sensing evidence. Companion reports of one cohort or device family were cross-referenced rather than treated as independent replication. Two separate axes were recorded: experimental setting (simulation; phantom/ex vivo; animal; human analytical specimen; prospective clinical event) and demonstrated function (target sensing, externally recovered target-dependent data, adjudicated recurrence). An unreported quantity is marked NR, an untested endpoint NT, and a tested negative result NEG; none may be substituted for another. A study can have human specimens but no in-body wireless experiment, so the axes must not be collapsed into one quality score. Table 2 summarizes the evidence classification used throughout the device comparisons.

Table 2. Evidence classification applied to device tables; a publication may occupy different levels for different functions. NR, not reported; NT, not tested; NEG, tested and negative.

Setting	Minimum Observable Evidence	Function to Record Separately
Simulation	Declared geometry, material, perturbation	Sensing response or calculated link only; no physical recovery
Phantom/ex vivo	Physical sample and reader/antenna arrangement	Target perturbation versus wireless target-feature recovery
Animal	Implanted device and stated follow-up	Biosensing, wireless delivery, and cancer event as distinct tests
Human analytical specimen	Patient-derived sample and assay/reference	Human-matrix target assay; not patient-level implanted validity
Prospective clinical event	Frozen rule, comparator, adjudicated follow-up	Event sensitivity, false-alert episodes, availability and lead time

3. Integration Classes and Clinical Endpoints

Table 3 defines the terminology used throughout. RF is a broad physical category: an inductively coupled resonator is not "non-RF", although it is different from a radiating GHz telemetry antenna. Likewise, a wirelessly powered optical implant can also contain Bluetooth RF communication. Power delivery, sensing physics, and data transmission must be classified separately. The classes describe functional roles and can overlap: for

example, a functionalized passive resonator combines molecular transduction with near-field interrogation. They are not mutually exclusive device categories.

Table 3. Integration classes used in this review. References identify the demonstrated sensing and readout roles; power, data, and transduction are classified separately.

Class	Signal Path and Examples	Evidential Boundary
A: tissue-loaded antenna	Tissue permittivity/conductivity changes antenna response [3,13,14].	The antenna is the transducer; dielectric contrast alone is not cancer-specific.
B: functionalized antenna	A recognition layer changes antenna impedance or resonance, as in the CEA sensor [4].	Molecular selectivity is possible; chronic in vivo assay performance remains unproven.
C: sensor plus implanted radio	An optical, electrochemical, or other sensor feeds implanted RF telemetry [5–7].	Cancer sensing and RF data delivery coexist, but the antenna need not be the selective element.
D: alternative implanted readout	The implant is read magnetically, optically, acoustically, or by near-field coupling [15–17].	Transferable biological/interface evidence; not equivalent to a radiating telemetry antenna.
Oral-access comparator	Tooth-mounted or removable oral sensors [18–20].	In-mouth is not necessarily tissue-implanted, and the demonstrated targets are not necessarily cancer markers.

Prediction, detection, and recurrence surveillance describe different clinical tasks. A molecular or physiological warning may precede conventional confirmation of an already developing tumour. Risk stratification estimates a probability of a future event; detection identifies present disease; recurrence detection concerns return after treatment; malignant transformation concerns progression of a precursor lesion; and a second primary is a new malignancy. These endpoints need different populations, time origins, reference standards, and thresholds. The present framework addresses measurements and warnings. A warning statistic becomes a recurrence-risk estimate only after calibration and independent validation for a defined population and time horizon. The framework does not establish prediction before a relevant biological change occurs.

4. Cancer Burden and the Surveillance Opportunity

Lung, colorectal, liver, breast, stomach, and pancreatic cancers contribute heavily to global mortality, but burden alone does not select an implant indication (Table 4). Figure 1 illustrates candidate site–specimen pairings; it does not depict clinically validated implanted surveillance. An oral mucosal lesion, a lung resection bed, and an ovarian/peritoneal implant create very different sampling and communication paths. A device's benefit depends on an accessible target, the frequency and location of clinically important events, and a feasible response to an alert.

Table 4. Selected global cancer deaths in 2022 and the corresponding surveillance design constraint [1].

Site	Deaths	Plausible Monitoring Niche	Dominant Constraint
Lung	1,817,172	High-risk postoperative/local monitoring	Motion, aeration, and distant relapse
Colorectum	903,859	Molecular or selected surgical-bed monitoring	Plasma ctDNA may not reach a local sensor
Liver	757,948	Post-resection/ablation surveillance	Cirrhosis, inflammation, multifocal disease
Female breast	665,684	Local recurrence; strongest device precedent	Scar response and distant relapse
Stomach	659,853	Local tissue or temporary GI sensing	Food/fluid loading and capsule transit
Pancreas	467,005	Selected postoperative research	Deep access and systemic recurrence
Brain/CNS	248,305	Resection-cavity monitoring	Necrosis, pseudoprogression, chronic safety
Lip/oral cavity	188,230	Mucosal or fluid-facing monitoring	Dilution, inflammation, biofilm, field disease

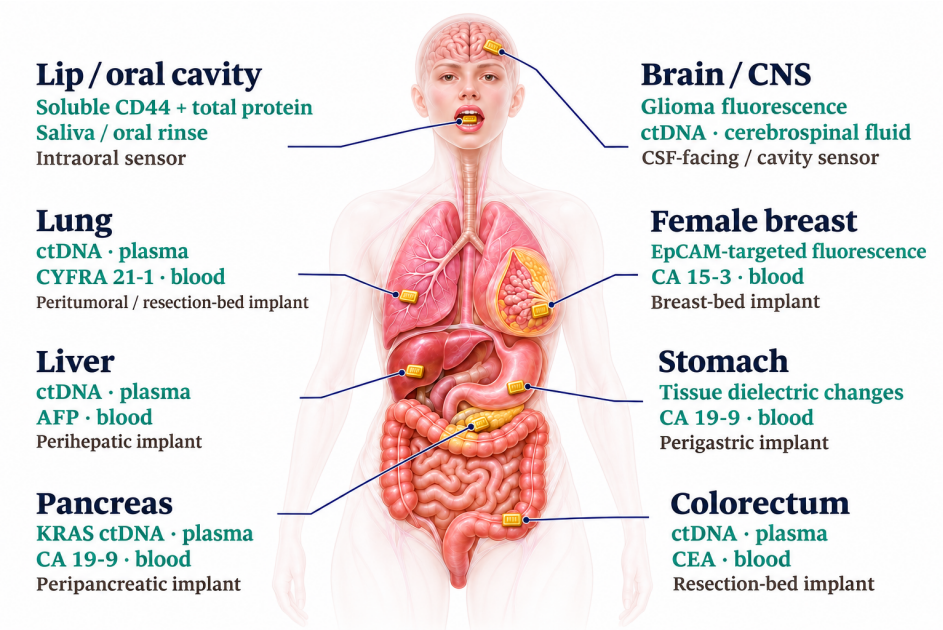


Figure 1. Conceptual illustration of selected anatomical sites, cancer-associated molecular markers, and optical or dielectric sensing approaches relevant to cancer surveillance. Examples of the underlying specimen- or device-specific evidence include oral-rinse CD44 [21,22], lung plasma ctDNA [23], glioma fluorescence [24], breast EpCAM sensing [7], and gastrointestinal antenna/capsule work [13]; see Tables 5 and 6 for the evidence boundaries. The listed fluids identify specimens used for biomarker measurements; detection in these fluids does not establish target availability at the illustrated implant site. The examples span clinical biomarker evidence, preclinical sensing approaches and proposed placements, rather than validated implanted surveillance systems. The image is a conceptual composition, not a reproduction of an externally published figure. CNS, central nervous system; ctDNA, circulating tumour DNA; CSF, cerebrospinal fluid; CD44, cluster of differentiation 44; CYFRA 21-1, cytokeratin 19 fragment; AFP, alpha-fetoprotein; EpCAM, epithelial cell adhesion molecule; CA 15-3, cancer antigen 15-3; CA 19-9, carbohydrate antigen 19-9; CEA, carcinoembryonic antigen.

Table 5. Priority-site translation map. Targets are evidence-backed; sensor–antenna combinations are testable proposals, not validated human recurrence systems.

Site/Endpoint	Evidence-Backed Target/Specimen	Candidate Sensing Route	Candidate In-Body RF Route	Decisive Experiment
Oral; recurrence and transformation assessed separately	Rinse CD44 and total protein; OPMD cytokine evidence [21,22,25]	Affinity panel + pH/temperature context	Submucosal radio with exposed/permeable sensing window	Paired device/laboratory values through healing, mucositis, inflammation, and incident disease
Oropharynx/ neck; regional recurrence	Plasma HPV DNA; postoperative lymph-fluid ctDNA [26,27]	Sequence-selective assay + local fluid access	Subcutaneous radio linked to a validated sampler	Target persistence after drain removal; regional versus distant event discrimination
Lung; postoperative recurrence	Serial tumour-informed plasma ctDNA [23,28,29]	Molecular assay only after local access is shown; physiology as context	Thoracic sensor + implanted RF or superficial relay	Paired local-fluid/plasma study with breathing and local/distant-event analysis
Breast; local recurrence	EpCAM fluorescence; dielectric contrast [3,7]	Optical affinity probe or functionalized RF surface + scar control	Optical–Bluetooth precedent or antenna-as-sensor	Probe renewal, phenotype coverage, benign controls, human longitudinal study

Table 6. Additional sites and anatomical constraints. No row implies an existing cancer-specific implant; RF band remains conditional on depth, loss, power, and packaging.

Site	Biomarker/Specimen Evidence	Candidate Sensor	Implant/RF Route	Main Gate
Stomach/GI	Tumour-oriented dielectric studies; gastric pH is non-specific [13,14,17]	Impedance or molecular surface; pH as context	915 MHz capsule precedent; fixed implant is distinct	Cancer versus gastritis/food/fluid loading; fixed coverage
Colorectum	Postoperative plasma ctDNA; site-agnostic CEA precedent [4,30,31]	Protein or sequence/methylation assay	Surgical-bed sensor + subcutaneous radio	Local transport, reagents, anastomotic inflammation, distant relapse
Ovary/ proximal compartments	HE4 biofluid assays; murine intraperitoneal sensing [16]	Antibody optical sensor; electrical coupling remains proposed	Optical precedent; human site must be validated before RF integration	Poor human peritoneal discrimination; select compartment, then test specificity, lifetime, and coverage
Brain/glioma	Glioma fluorescence concept [24]; transferable oxygen-implant safety from superficial skin/breast tumours [32]	Optical sensor; oxygen only with glioma-specific validation and treatment-effect controls	Cavity sensor linked to subscalp electronics	Label availability, necrosis or pseudoprogression, and site-specific chronic safety
Liver	Serial plasma ctDNA and HCC recurrence [33]	Sequence-selective sensing	Local sensor + RF relay	Cirrhosis, multifocal disease, fluid access, deep link
Pancreas	Portal/peripheral KRAS ctDNA [34]	Mutation-specific assay with preparation	Surgical-bed sampler + implanted radio	Interstitial access and distant-disease coverage
Bladder	Longitudinal urine tumour-DNA patterns [35]	Urine-contact nucleic-acid assay + ionic/pH correction	Candidate intravesical sensor–RF system	Encrustation, infection, retention, benefit over voided urine

In Europe, the Joint Research Centre's EU-27 factsheet estimated approximately 1.3 million cancer deaths in 2024, with lung, colorectal, pancreatic, and breast cancers among the leading causes [36]. The European burden supports prioritizing lung and other lethal malignancies, while oral/head-and-neck disease is compelling because local sampling may be more practical than deep implantation.

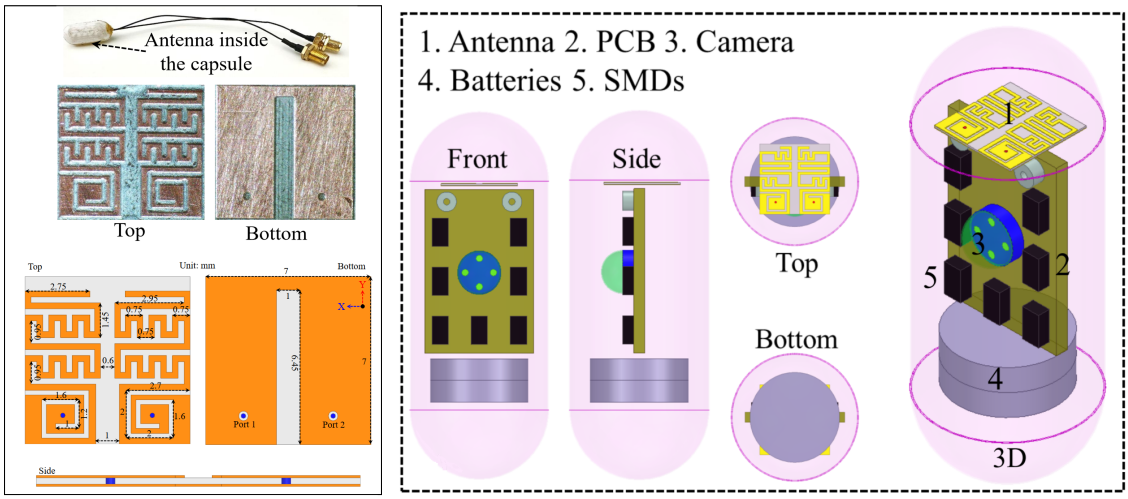
Residual or dormant disease also creates an important negative result: absence of a local signal is not evidence that all cancer has been eliminated. Quiescent or low-shedding cells may generate little target, and disseminated disease may lie outside the sampled region [2]. Early-warning claims must therefore specify local, regional, or systemic coverage. Clinical benefit further requires an effective action after a warning. The ALTAIR trial in ctDNA-positive colorectal cancer illustrates this separation: molecular selection did not ensure that the tested early treatment improved the primary disease-free-survival endpoint [37]. Surveillance technology must be evaluated as part of a management pathway, not solely as a more sensitive instrument.

5. Cancer-Facing Antenna and Implant Systems

5.1. Dielectric-Response Antenna Sensors

Wang et al. provide a direct precedent for the proposed antenna-as-a-sensor concept [3]. Their 2.45 GHz implanted antenna responds to surrounding tissue dielectric properties; the reported resonance change is approximately 9–18 MHz for a ten-unit permittivity increase in the studied conditions. Measurements in tissue-mimicking media

support an electromagnetic sensing mechanism. However, the experiment does not establish longitudinal discrimination of malignant recurrence from postoperative oedema, scar maturation, inflammation, or fluid changes. Its central contribution is a compact local dielectric-sensitive RF interface, not a validated recurrence test. Smida et al. and Smida extend the tissue-sensitive concept to compact 915 MHz MIMO structures motivated by gastrointestinal monitoring [13,14]. Resonance varies with the surrounding permittivity while communication-oriented quantities are assessed. These are important non-breast examples. Their cancer relevance is nevertheless inferential: a parameter sweep of tissue dielectric properties is not a study of histologically verified early gastric cancer. A moving capsule also lacks the fixed position, repeated access to the same tissue, and long-term interface of a surveillance implant. Kagitha et al. combine a frequency-reconfigurable antenna with machine learning analysis of scattering data [38]. Their breast-model figure describes the antenna as mounted on the surface, whereas tissue-gel measurements demonstrate the antenna's implant-oriented RF characteristics. The tumour-classification experiment should therefore not be counted uncritically as a wholly implanted cancer-sensing chain. Figure 2 shows the antenna geometry and capsule packaging reported in the two studies [13,14].



(**a**) (**b**)

Figure 2. Two 915 MHz gastrointestinal capsule-antenna studies. (**a**) Photograph of the capsule-mounted prototype and top/bottom antenna geometry, assembled from Figures 1 and 8a of Smida et al. [13] (copyright 2025 the authors, CC BY 4.0). (**b**) Modelled capsule layout with antenna, printed circuit board, camera, batteries, and surface-mounted devices, cropped from Figure 2b of Smida [14] (copyright 2026 the author, CC BY 4.0). Both panels have been cropped and rearranged under the respective articles' Creative Commons Attribution 4.0 licenses (https://creativecommons.org/licenses/by/4.0/ (accessed on 15 October 2026); https://www.mdpi.com/1424-8220/25/11/3323 (accessed on 15 October 2026); https://www.mdpi.com/1424-8220/26/5/1694 (accessed on 15 October 2026)); neither demonstrates cancer-recurrence detection.

5.2. The CEA Antenna Immunosensor

Chen et al. most closely match a molecularly selective implanted antenna sensor [4]. An Au-nanoparticle-decorated graphene layer on a compact radiating patch is functionalized for CEA recognition. The reported device dimensions are $5 \times 3 \times 0.127$ mm^3, and the response over 0.01–100 ng/mL has a magnitude of approximately 2.46 MHz per decade of concentration. The important advance is the biochemical-to-RF interface: antigen recognition changes the antenna's electrical response, instead of treating every tissue-loading change as evidence of cancer.

Concentration-dependent far-field gain was also measured under cabled excitation, and a three-layer simulation yielded a peak 1 g SAR of 1.57 W/kg at an input power of 1.8 mW [4]. These are reported radiation and exposure results, not evidence of untethered, through-tissue biomarker recovery or chronic recurrence monitoring. The simulation does not establish device-specific compliance under present-day operating conditions.

Its assay conditions delimit the conclusion. The preparation includes antibody incubation, blocking, antigen exposure, washing, and drying. Human-serum recovery experiments use serum diluted to 5% in a buffer; the reported recoveries are 93.5–100.2%. A month-long stability test under controlled immunoreactivity conditions is not a month of continuously implanted function. Similarly, a short, controlled concentration experiment does not establish that a binding surface can follow rising and falling CEA in vivo without saturation or regeneration. These distinctions are essential when designing a chronic warning device.

The reported low analytical detection limit should also be distinguished from the measured calibration range. For a response fitted against $\log_{10} C$, a slope in MHz/decade cannot be inserted into 3σ/slope and interpreted directly as a concentration without an appropriate inverse calibration and blank model. The measured range and reported slope are therefore used to discuss transduction; the extrapolated limit is not treated as evidence of clinical early detection. CEA itself is not specific to one tumour site or exclusive to malignancy; the appropriate comparator is a site- and population-matched clinical assay. The paper establishes a valuable Class-B precedent while leaving the chronic biological interface and recurrence endpoint open. Table 7 states the corresponding evidential boundaries.

A subsequent eight-channel Au–vertical-graphene antenna array extended this laboratory concept to rapid CYFRA 21-1 detection in human serum, using an RF switch to address the sensing elements [39]. At 2.45 GHz, the authors reported microwave-assisted self-incubation and used a temperature controller to hold the array at 37 °C; response times of approximately 2 min (single element) and 5 min (array) therefore belonged to those excitation and thermal conditions, not to an unpowered implanted surface. This study strengthens the case for multiplexed molecular-to-RF transduction, but its demonstrated context is a prepared multichannel serum assay rather than a chronically implanted, wireless body-to-reader system. Multiplexing therefore addresses marker coverage only after sampling, regeneration, packaging, and in-body interrogation have been established.

For Class B, recovery means that a reader outside the body measures the target-dependent resonance, phase, or backscatter feature through the final wet package and tissue. A cable-connected VNA establishes laboratory transduction, not this recovery. For a passive Class-D resonator, the external coil measures a reflection or coupling feature that depends on both the sensing element and mutual inductance; reader displacement and orientation must be crossed with target levels rather than held fixed. Class C's digital radio instead needs calibrated sensor values, valid packets, known timestamps and delivery within the event window; no biomarker-driven change in carrier frequency is required. Table 8 gives the minimum discriminating experiment for each route.

Table 7. Quantitative comparison of antenna-centred sensing studies. NR: not reported; VNA: vector network analyser. A far-field radiation test is not counted as wireless recovery of the concentration-dependent sensing feature.

Band/Evidence	Sensing/Readout Arrangement	Implant/Test Geometry	Time/Read Evidence	Evidential Boundary
2.45 GHz [3]	Tissue permittivity → f_r; SMA/VNA sensing measurement	5 × 5 × 0.528 mm^3; 30 mm tissue phantom/pork depth	No longitudinal service test; 0.8 m horn test assessed radiation only	Local dielectric response demonstrated; no malignant-versus-healing or reader-level warning
2.45 GHz [4]	Au–graphene CEA binding → f_r; 50 Ω cable/VNA; cable-fed gain vs CEA	5 × 3 × 0.127 mm^3 exposed-liquid assay; implant depth NR	300 min response experiment; one-month controlled stability; untethered through-tissue recovery NT	Direct molecular antenna transduction; chronic undiluted-matrix operation unproven
2.45 GHz [39]	Eight Au–vertical-graphene antenna channels and RF switch; CYFRA 21-1 in serum	Laboratory multichannel assay; implant geometry/depth NR	2/5 min with microwave-assisted incubation and 37 °C control; chronic reads NR	Rapid multiplexable antenna assay, not demonstrated as an implanted body-to-reader link
915 MHz [13,14]	Capsule MIMO; surrounding-permittivity response and communication metrics	GI/capsule-oriented tissue models and prototypes	Fixed-site duration and read availability NR	Useful telemetry/sensing co-design; tumour-specific and fixed-site validation absent
1.4/2.4 GHz [38]	Reconfigurable antenna; scattering features with machine learning	Implant-oriented tissue tests, but surface-mounted antenna in the classification model	Independent longitudinal reads NR	Classification result cannot yet be treated as a wholly implanted cancer-sensing chain

Table 8. Architecture-specific external-reader evidence. NR is an unavailable quantitative result, not a negative experimental finding. Depth is implant-to-surface distance, whereas reader separation is implant-to-reader distance.

Route/Precedent	Externally Measured Quantity	Reader, Tissue and Power Test Needed	Status of Key Link Quantities
Class A, 2.45 GHz [3]	Uncabled resonance/scatter change vs dielectric target	Declared 30 mm phantom/pork depth; cross tumour-like load with tissue/reader displacement; document polarization, loss, margin, input power and SAR	Radiation assessed with a horn at 0.8 m; wireless target feature, longitudinal availability and cancer specificity NT
Class B, 2.45 GHz [4]	Reader-resolved Δf_r or differential backscatter vs CEA	Wet selective window, sealed radiator/feed, stated depth and external reader angle; independently vary CEA, temperature, salt, coupling and reference	Cabled calibration and CEA-dependent far-field gain measured; simulated 1 g SAR 1.57 W/kg at 1.8 mW. Untethered through-tissue CEA recovery NT; its reader geometry, SNR/margin and read availability NR.
Class D, passive LC [9,17]	External-coil resonance or phase relative to blank resonator	Report coil separation/orientation, Q, load dependence, reader power, tissue and package; repeat target and displacement factorially	Passive wireless pH shown for noncancer endpoint; cancer-target recovery and recurrence NT
Class C, 13.56 MHz WPT + BLE [5,6]	Decoded optical value, packet error/time stamp	Report reader power/duty cycle, depth, separation, orientation, valid-packet fraction and safety in worst-case geometry	Implanted rodent optical telemetry demonstrated; human recurrence discrimination NT; prospective valid-read fraction NR

5.3. Cancer Biosensors with Implanted RF Telemetry

Cancer-related optical transduction does not exclude an RF antenna elsewhere in the same implant. Kim et al. combined optical tumour-size monitoring and treatment in a flexible implant using inductive power and Bluetooth communication, including a mouse xenograft model and multiweek implantation [5]. Nie et al. used an optical oxygen-saturation channel, a 13.56 MHz wireless-power interface, and Bluetooth telemetry to distinguish and monitor tumour-associated conditions in preclinical experiments [6]. Oxygen saturation is not identical to interstitial oxygen partial pressure; vascular physiology and optical conditions affect the interpretation. Nevertheless, both papers materially connect implanted cancer sensing with RF data delivery.

Weng et al. are especially close to the broader recurrence-monitoring brief [7]. Their device uses an EpCAM-targeting fluorescent DNA probe, optical excitation, a photoresistor, ultrasound energy harvesting, and a Bluetooth low-energy system-on-chip. Thus, ultrasound supplies power while an RF link carries data. The paper reports animal local-recurrence experiments, including detection at an approximately 3 mm recurrent tumour size. The limits are as informative as the integration. Targeted probes were administered in the experimental workflow; the result is not a reagent-free indefinite implant. Normalized fluorescence trajectories distinguish the experimental groups, but a deployment algorithm needs a fixed prospective calibration rather than a normalization requiring an animal's future extrema. The animal finding does not establish sensitivity for naturally occurring human recurrence, a universal minimum tumour size, or specificity across tumour phenotypes. This study is therefore a relevant preclinical recurrence-monitoring precedent with RF telemetry, while probe supply and prospective human validation remain open.

5.4. Alternative Readout and Transferable Sensing Mechanisms

Daniel et al. demonstrated access to a local cancer-related biomarker through an implanted magnetic-relaxation device in tumour-bearing animals [15]. Williams et al. developed an antibody-functionalized optical nanotube implant for the ovarian marker HE4, with intraperitoneal measurements through 24 h in four murine ovarian-cancer models [16]. This establishes local molecular sensing with external optical interrogation. The authors also caution that human peritoneal HE4 may provide poor diagnostic discrimination at that location; the animal result therefore does not establish a clinically suitable human implantation compartment. Schaufler et al. proposed a glioblastoma recurrence-monitoring system with a resection-cavity optical module, a connected subscalp electronics module, and wireless energy/readout engineering; optical feasibility was studied in phantoms and porcine brain tissue [24]. Together, these studies show how cancer-facing implants differ in anatomical access, readout architecture, and validation stage.

Jo et al. investigated a hydrogel responsive to pH and ROS that converts cancer-microenvironment conditions into electrical changes [40]. Li et al. coupled pH-responsive material to a passive wireless resonator for gastric leakage, not cancer [17]. Corsi et al. demonstrated an implanted optical sensor for local doxorubicin pharmacokinetics [41]; drug exposure was a treatment measurement, not proof of tumour recurrence. Such work supplies transducer and interface principles, provided its actual target is retained. The synthesis is that biological recognition, chronic exposure, and radio readout each have precedents, but their successful combination depends on the particular organ and endpoint. Table 9 keeps the sensing mechanism, power link, data path, and evidence level distinct.

Table 9. Cancer-facing implanted systems and adjacent mechanisms. Sensing, power, and data paths are separated. NR: not reported; "no RF data" means that the cited sensing experiment did not demonstrate a radiating-RF telemetry path.

Signal/Transducer	Power and Data	Placement/Link Test	Duration/Reads	Evidence Boundary
hCG-β; magnetic relaxation [15]	External magnetic-resonance interrogation; no RF data	Implanted sensing material in tumour-bearing mice	Longitudinal read availability NR	Local molecular access shown; not antenna telemetry
HE4; antibody/nanotube optical response [16]	External optical interrogation; no RF data	Intraperitoneal membrane-encapsulated sensor in mice	Four ovarian-cancer models; reads through 24 h; chronic functional lifetime unestablished	Local sensing shown; human peritoneal diagnostic discrimination remains a concern
Scattered-light estimate of tumour size [5]	13.56 MHz inductive power; BLE data	Fully subcutaneous mouse implant near/in xenograft; smartphone receiver	2–3 weeks; generally weekly measurements; some early termination from operational difficulty	Complete cancer-sensor/RF chain, but treatment-response monitoring rather than recurrence validation
Fluorescent glioma tissue [24]	Wireless-power/readout concept; intermodule cable	Resection-cavity optical head plus subscalp electronics; phantom and porcine tests	Chronic in vivo duration/read availability NR	Anatomically explicit recurrence concept; prospective event detection absent
Optical sO_2 (oxygen saturation) [6]	13.56 MHz inductive power; BLE data	Subcutaneous rodent implant; more than 60 mW received at 5 cm coil separation	10-day therapy study; tissue response reported to day 15; usable-read fraction NR	Tumour/therapy physiology monitored; sO_2 is not a molecular recurrence marker
EpCAM-targeted fluorescence [7]	1 MHz ultrasound power; BLE data	Subcutaneous rat implant; operation through 20 mm porcine muscle and energy harvesting tested up to 48 mm	Three-week safety assessment; diagnostic-cycle reads; availability fraction NR	Animal local recurrence at ~3 mm; injected probe, calibration, and human specificity remain unresolved
pH/ROS hydrogel; electrical state [40]	No implanted RF telemetry	Material/sensor study	Chronic service NR	Cancer-microenvironment transducer only
Gastric-leakage pH [17]	Passive wireless LC resonator	Bioresorbable implanted sensor; external near-field readout	Continuous pH study over the reported resorption/use window	Transferable pH and packaging method; endpoint is not cancer
Local doxorubicin; optical sensor [41]	Optical interrogation; no RF data	Implantable bioresorbable optical sensor	In vivo pharmacokinetic monitoring; RF read availability NR	Treatment-exposure measurement, not tumour recurrence

6. Biomarkers, Biosensors, and the Measurable Cancer Interface

6.1. Molecular Identity and Local Physiology

Cancer-associated changes fall into complementary categories. Proteins such as CEA, HE4, soluble CD44, and cytokines can be recognized by antibodies, aptamers, or related affinity layers. Nucleic-acid targets include tumour-informed mutations, methylation signatures, viral tumour DNA, and selected RNA profiles. Their disease attribution can exceed that of a bulk physiological variable, but recognition, molecular sampling, and often processing are more demanding. Physiological measurements—pH, oxygenation, ROS, impedance, conductivity, temperature, pressure, and strain—can offer simpler continuous transduction while responding to many benign processes.

A useful design does not treat these categories as interchangeable. An antibody supplies molecular binding specificity, not automatically specificity for malignant recurrence. A low-pH measurement supplies a local chemical observation, not tissue identity. Pressure can reflect obstruction, oedema, healing, or tumour mass and should not be promoted as an established early cancer marker merely because passive pressure sensors exist [9,42]. A molecular channel plus selected physiological context is a testable strategy for improving interpretation; its benefit must be shown against a molecular-only baseline.

6.2. Clinical Association Is Not Implant Feasibility

Serial plasma ctDNA has substantial recurrence-association evidence in lung, head-and-neck, and colorectal cancer [23,30,43]. Salivary proteins and cytokines have clinical association and risk-stratification evidence in oral disease [21,25]. These studies establish targets in collected specimens. They do not show that the same target is present at a buried antenna at the same concentration, that a continuously exposed surface can regenerate, or that every measurement can be read wirelessly.

Conversely, biosensor papers establish analytical mechanisms under stated conditions. Wei et al. demonstrated simultaneous electrochemical IL-8 mRNA and protein detection in saliva, including 28 cancer and 28 control specimens [44]. Torrente-Rodríguez et al. studied dual magnetobiosensing in raw saliva, including spiked measurements and endogenous protein measurements in healthy volunteers [45]. Those are different evidential designs. Labelled reagents, magnetic beads, incubation, washing, and amplification may be appropriate for laboratory assays but cannot be assumed to fit an unattended implant. Table 10 therefore preserves each study's specimen, cohort, and endpoint.

Table 10. Selected clinical and analytical anchors. Each result applies only to its stated specimen and endpoint; none is implant performance.

Specimen/Cohort	Reported Result	Supports/Does Not Support
Saliva, 28 cancer/28 control [44]	IL-8 mRNA LOD 3.9 fM; protein LOD 7.4 pg/mL; ~90% sensitivity/specificity in that dataset	Multiplex feasibility/not prospective recurrence or chronic use
Raw saliva, spiking and 7 healthy participants [45]	LOD 0.21 nM mRNA and 72.4 pg/mL protein	Matrix-compatible assay/not cancer-cohort discrimination
172 treated oral/oropharyngeal patients [21]	36 recurrences; CD44 and total protein associated with recurrence risk	Endpoint-relevant association/no implanted threshold
1313 saliva samples, 749 longitudinal OPMD cases [25]	IL-6-based ratios/indices associated with malignant transformation	Risk-panel evidence/not deterministic prediction or recurrence
197 NSCLC patients, 1069 plasma samples [23]	Landmark ctDNA identified 49% of eventual relapses; serial sampling added events	Longitudinal comparator/plasma processing and low shedding remain

Table 10. *Cont.*

Specimen/Cohort	Reported Result	Supports/Does Not Support
76 plasma/54 saliva patients [43]	Plasma (≥14 days post-surgery): 21/23 recurrences; median lead time 119 days (14–500); specificity 94.2%	Endpoint-specific: both second-primary tumours were missed; plasma performance is not saliva performance
1039 resectable colorectal cases [30]	Four-week ctDNA positivity: recurrence HR 10.0	Prognostic value/not implant feasibility or treatment benefit
243 ctDNA-positive randomized patients [37]	Primary DFS endpoint not met (HR 0.79; $p = 0.107$)	Early warning and beneficial intervention are separate hypotheses

6.3. RF-Compatible Transduction and Its Service Requirements

The CEA antenna demonstrates direct recognition-layer loading [4]. Lei et al. provide an additional microwave CEA biosensor and classification precedent [46]; Chen et al. extend antenna immunosensing to an eight-channel CYFRA 21-1 serum assay [39]; and Montoya-Villada et al. demonstrate a microstrip immunosensor for anti-p53 autoantibodies [47]. None should be relabelled a chronic implanted surveillance system. Collectively, they show that molecular recognition can modulate microwave observables and that antenna arrays can support rapid multichannel assays. Translation still requires in-body matrix calibration, packaging, regeneration, and reader-level recovery of the biomarker-dependent feature.

Electrochemical interfaces offer another route: a selective electrode can control a tunable load or feed an RF transceiver. A pH/ROS-sensitive hydrogel can change impedance, geometry, or dielectric loading [17,40]. An optical target can be digitized and transmitted, as already demonstrated in the cancer-facing systems above. These routes differ in power, interrogation distance, multiplexing, and serviceability. An irreversible capture surface is closer to an accumulating dosimeter unless renewal or dissociation is established; a true concentration tracker must respond appropriately to both increases and decreases.

Recognition layers impose different service-life limits (Table 11). Report separately the chemical lifetime, effective measurement lifetime, implanted duration, and proportion of scheduled reads successfully acquired. A one-month stability test after laboratory preparation cannot establish any of the latter three. An exposed target window must admit the molecule while a continuous hermetic barrier protects the feed, electronics, and power conductors; complete encapsulation of the receptor would block the analyte.

Table 11. Recognition and service requirements. The evidence column states what was demonstrated; no service interval is extrapolated from a short assay.

Interface	Dominant Failure or Renewal Issue	Existing Demonstration/Missing Chronic Test
Antibody capture [4]	Saturation, irreversible retention, fouling and antibody loss; renew or replace surface	Washed/dried CEA assay and controlled stability; repeatable wet in vivo tracking NT
Reversible affinity [48,49]	Off-rate sets recovery; diffusion and fibrosis restrict replenishment	Kinetic principle; required in vivo rise/fall cycles and service life target-specific
Electrochemical [50,51]	Electrode drift, reference depletion, contamination and biofouling	Oral-cancer fluid assay and wireless glucose precedent in different settings; cancer-specific repeatable implant NT
Optical probe [7,16]	Photobleaching, probe supply, tissue opacity and membrane transport	Animal/short-term sensing and animal recurrence shown; indefinite reagent-free operation NT

7. Body-Site Evidence and Candidate Sensor–Antenna Combinations

Tables 5 and 6 distinguish the measured clinical specimen from the proposed implant compartment. "Candidate" indicates a research hypothesis. A CEA antenna's existence does not validate lung, colorectal, or pancreatic recurrence simply because those diseases can involve CEA. Likewise, an antenna can be implanted close to an organ without sampling the relevant fluid. Paired biological sampling is often the first experiment needed to establish whether RF integration is justified.

The value of implantation therefore depends on the clinical setting. In bladder disease, easily collected urine may make an implanted assay unnecessarily burdensome. In deep lung, pancreatic, and liver sites, a molecular target may be accessible in blood but not at the proposed implant. Oral platforms may permit easier maintenance, although they are not automatically tissue-implanted. Two distinct research uses are prioritized in Table 12: an oral, local-event system with a potentially serviceable fluid-facing surface, and a thoracic surgical-bed feasibility study for which local molecular access must first be demonstrated. This conclusion is an engineering inference from the evidence map, not a clinical recommendation.

The oral use case does not justify surgery if home saliva/rinse collection supplies equally reliable and timely information. The lung use case remains a biological-access study, not a proposed clinical implant indication; a chest-wall radio cannot sense circulating tumour DNA merely by proximity. In both, the clinical action after a positive warning and the harm of an unnecessary work-up must be specified before choosing the acquisition rate.

Table 12. Prioritized hypotheses; an implant proceeds only if it offers a measurable advantage over an accessible test. Targets and performance from the cited specimens are not assigned to the proposed implant.

Indication/Evidence	Placement, Sample, Clinical Endpoint	Comparator and Potential Incremental Value	Boundary and First Decisive Test
Oral post-treatment local recurrence [21,52]	Replaceable mucosa-facing molecular window, radio in adjacent protected submucosal site; mucosal fluid/saliva; biopsy-confirmed local recurrence	Scheduled oral rinse, examination and biopsy; added value only if frequent unattended valid monitoring gives an earlier actionable warning at acceptable false-alert burden	Oral-rinse concentrations cannot be borrowed for mucosal film; paired fluid/interface assays through healing, infection and recurrence before implanting
Lung post-resection local relapse (conditional) [23,28]	Proposed pleural/resection-bed fluid interface with protected subcutaneous relay; imaging/pathology-confirmed local relapse	Plasma ctDNA and standard imaging; remote or distant recurrence is outside local coverage unless separately accessed	Plasma ctDNA evidence does not prove pleural access; first obtain paired local-fluid/plasma and benign postoperative samples and quantify event-location frequency

Lung and Head-and-Neck Surveillance as Distinct Design Problems

TRACERx shows the value and limitations of serial plasma measurements in NSCLC [23]. Gale et al. further show that postoperative sampling timing matters [28]. A chest-wall antenna, even if it communicates reliably, does not acquire plasma ctDNA simply by being near the lung. A thoracic implant for pH or oxygen can reasonably investigate a local physiological trajectory, but that is a new surrogate-validation study. Respiratory motion, aeration, resection-related fluid, and pleural changes must be modelled as potential signal sources rather than only RF disturbances.

Head-and-neck molecular surveillance is more anatomically differentiated than the label suggests. Chera et al. studied tumour HPV DNA in plasma for HPV-associated

oropharyngeal cancer [26]; that target cannot be generalized to HPV-negative oral cancer. Earland et al. demonstrate a proximal postoperative lymphatic-fluid opportunity [27], but a temporary surgical drain does not prove a stable fluid compartment exists months later. Flach et al. distinguish plasma and saliva sampling in surgically treated HNSCC [43]. Together, these studies support site-specific pairing of target, accessible compartment, and recurrence pattern; they do not support a universal neck implant.

The corrected Chera article and its 2023 erratum must be interpreted together [26]. Consent-related exclusions reduced the evaluable cohort from 115 to 45 patients; reanalysis widened confidence intervals without changing the main conclusions. Superseded performance estimates from the original cohort are not used here.

8. Oral Cancer: Salivary Markers, pH, and the Intraoral Interface

8.1. Endpoint-Matched Molecular Channels

The oral cavity is especially attractive because biological exposure and external reader access can be relatively direct. However, whole saliva, an oral rinse, the mucosal film, gingival crevicular fluid, and tooth biofilm are different matrices. Marker recovery at a tooth surface may be affected by local flow, adsorption, food, and biofilm. A validated oral-rinse threshold must therefore be re-established at the actual device interface.

Bastías et al. reviewed a large candidate salivary biomarker space and highlighted cytokines, LDH, and MMP-9, while emphasizing the need for larger clinical studies [12]. For recurrence, CD44 and total protein merit particular attention because the evidence includes treated patients followed for recurrent disease [21]. Raslan et al. provide a prospective high-risk cohort rather than a postoperative recurrence cohort [22]. Neither establishes a universal threshold, and total protein should not automatically be used as an inert dilution denominator when it can carry disease-related information itself.

For emergence from an oral potentially malignant disorder (OPMD), Chen et al. provide a contemporary longitudinal anchor [25]. IL-6, IL-6/IL-1Ra, and a composite cytokine index were associated with malignant transformation. A hypothesis for implant-supported monitoring can therefore begin with a measured cytokine panel and explicit inflammation controls rather than salivary acidity alone. Nonetheless, an association in a defined cohort does not prove reliable prediction for every lesion or transfer to a continuously exposed recognition layer.

Salivary miR-423-5p and tumour-related DNA provide additional identity-bearing channels [52–54]. Their practical difficulty is not RF transmission but obtaining sufficient molecules and maintaining reliable sequence recognition. CYFRA 21-1, IL-8, and p53-oriented immunosensors demonstrate additional analytical possibilities in serum and saliva [50]. These should be selected for complementary evidence and feasibility, not to maximize the number of targets in a diagram. Table 13 summarizes the resulting oral channels, interface needs, and main confounders.

Table 13. Practical oral-channel map. Each proposed role is a hypothesis, not an endorsed diagnostic panel.

Channel	Evidence	Interface Requirement	Proposed Role/Main Confounder
CD44 + total protein	Recurrence/high-risk associations [21,22]	Separate calibration, selective capture, renewal	Local warning/inflammation, dilution
IL-6, IL-8, IL-1Ra	OPMD transformation; IL-8 sensing [25,44,45]	Multiplex selectivity, matched matrix, replaceable/reusable layer	Risk panel/oral inflammation
CYFRA 21-1/p53 antigen/anti-p53 autoantibodies	Human-fluid immunosensor feasibility [39,47,50]	Separate capture chemistry and calibration for antigen and autoantibody targets	Complementary markers/limited longitudinal evidence
miRNA/tumour DNA	Diagnostic/prognostic and serial studies [52–54]	Sequence control, sample volume, processing	Molecular identity/low abundance and nuclease effects
pH/conductivity	Salivary and in-mouth variation [55,56]	Spatial calibration; food/biofilm controls	Context/quality/non-specificity
Temperature/impedance	Oral RF and lesion-impedance evidence [19,57]	Stable contact; thermal/fluid correction	Adjunctive change/contact and benign tissue effects

8.2. Salivary Acidity and Tumour Extracellular Acidity

Tumour extracellular acidity is not equivalent to salivary acidity. Spatially localized pericellular acidity can differ greatly from a bulk-fluid measurement [58]. Whole saliva is buffered, mixed, and strongly affected by flow, diet, oral microorganisms, and treatment. A pH-sensitive element in a biofilm and one facing the mucosa can therefore report different trajectories without either being faulty.

Available clinical evidence does not justify a universal "lower salivary pH means cancer" threshold. Shpitzer et al. reported median saliva pH of 7.0 in 25 tongue-OSCC patients versus 6.4 in 25 controls [55]. The direction itself cautions against translating the acidic tumour-microenvironment concept directly to whole saliva. Geiken et al. measured saliva and biofilms continuously over 96 h in 12 participants and documented glucose-related and compartment-dependent pH changes [56]. That study supports feasible longitudinal context measurement, not cancer discrimination.

The practical hypothesis is thus to use pH alongside a clinically grounded molecular channel, recording whether pH explains matrix drift or adds independent cancer information. A useful negative outcome would be that pH improves measurement quality but does not improve event discrimination. This is scientifically preferable to assigning cancer specificity to an easily measured variable.

8.3. Oral Wireless Interfaces and the Implant Distinction

Mannoor et al. coupled graphene and peptide recognition to a tooth-mounted wireless resonant platform for bacteria sensing [18]. Tseng et al. demonstrated tooth-mounted RF-trilayer sensing of the oral environment and food-related exposures [19]. Ahmad et al. studied a flexible loop reader coupled to LC sensors, using artificial saliva and other test liquids to characterize dielectric response [20]. These papers provide valuable oral access, mechanical, and wireless-coupling methods. None establishes selective cancer recurrence detection merely because saliva is part of the experiment.

A tooth-mounted patch, removable mouthguard, and buried mucosal implant also differ in biological exposure and service. A replaceable oral sensing layer may be a more credible first research platform than permanently burying an irreversible assay. A fixed implanted radio could, in principle, interrogate a serviceable exposed sensor, but that separation introduces contamination, connection, and mechanical requirements. The choice should follow comparative benefit and maintenance evidence.

9. Translational Design and Validation Framework

9.1. Architecture

The proposed hypothesis is deliberately narrow: for a defined anatomical site and follow-up endpoint, a target channel combined with context and a nonrecognizing reference can provide a more interpretable implanted warning than an unreferenced dielectric shift. The target channel supplies disease-related information; context channels such as pH, temperature, conductivity, oxygenation, or motion explain changes that may alter the sensor without being cancer; and the reference channel measures common drift without intentionally binding the target. This arrangement does not make a nonspecific marker cancer-specific, but it creates a testable way to separate biological signal from benign loading and device drift.

Figure 3 organizes three implementation routes. A functionalized antenna may convert binding directly into impedance, resonance, or backscatter, as demonstrated for CEA [4]. A separate optical or electrochemical transducer may be digitized and transmitted through an implanted radio, as in existing cancer-facing systems [5–7]. A passive near-field resonator is also possible when coupling depth and reader geometry are acceptable [9,17]. Power delivery, data communication, and sensing physics are specified separately in every route.

Figure 4 makes the representative Class-B interface explicit. The fluid reaches only the selective recognition window and a nearby nonbinding reference window; the feed, passives, and any active electronics remain sealed. A selective membrane is not a freely permeable hermetic seal: its permeability and thickness control analyte arrival, while its dielectric properties and the local fluid alter resonance. The reference should share that membrane, tissue and reader environment without sharing specific target binding. Its coefficient κ is estimated from independent benign challenges, and retained target sensitivity must be measured again after subtraction. For a real implant, membrane fouling and foreign-body encapsulation modify both sampling and RF boundary conditions.

A design should also specify implantation volume and surgical route, migration fixation, sterilization effects on affinity chemistry, leak testing, replacement/explantation, and tissue reaction during the proposed service interval. RF and wireless-power tests need final packaging, a declared worst-case orientation, tissue-dependent detuning/loss, input/duty-cycle and local temperature or SAR evaluation against applicable frequency-specific limits [59]. Exposing the recognition window and sealing the electronics are competing requirements; a fully sealed receptor is inaccessible, and an unsealed feed is not a chronic implant.

The central hypothesis should be specified before hardware development: at the same false-alert burden and usable-read requirement, the complete target–context–reference system detects a specified event better than target-only, dielectric-only, and routine-follow-up comparators. A second claim can test whether a functionalized antenna retains target information after benign loading, reader displacement, temperature change, and biointerface drift. Failure to outperform these comparators is informative and should stop or redirect the design.

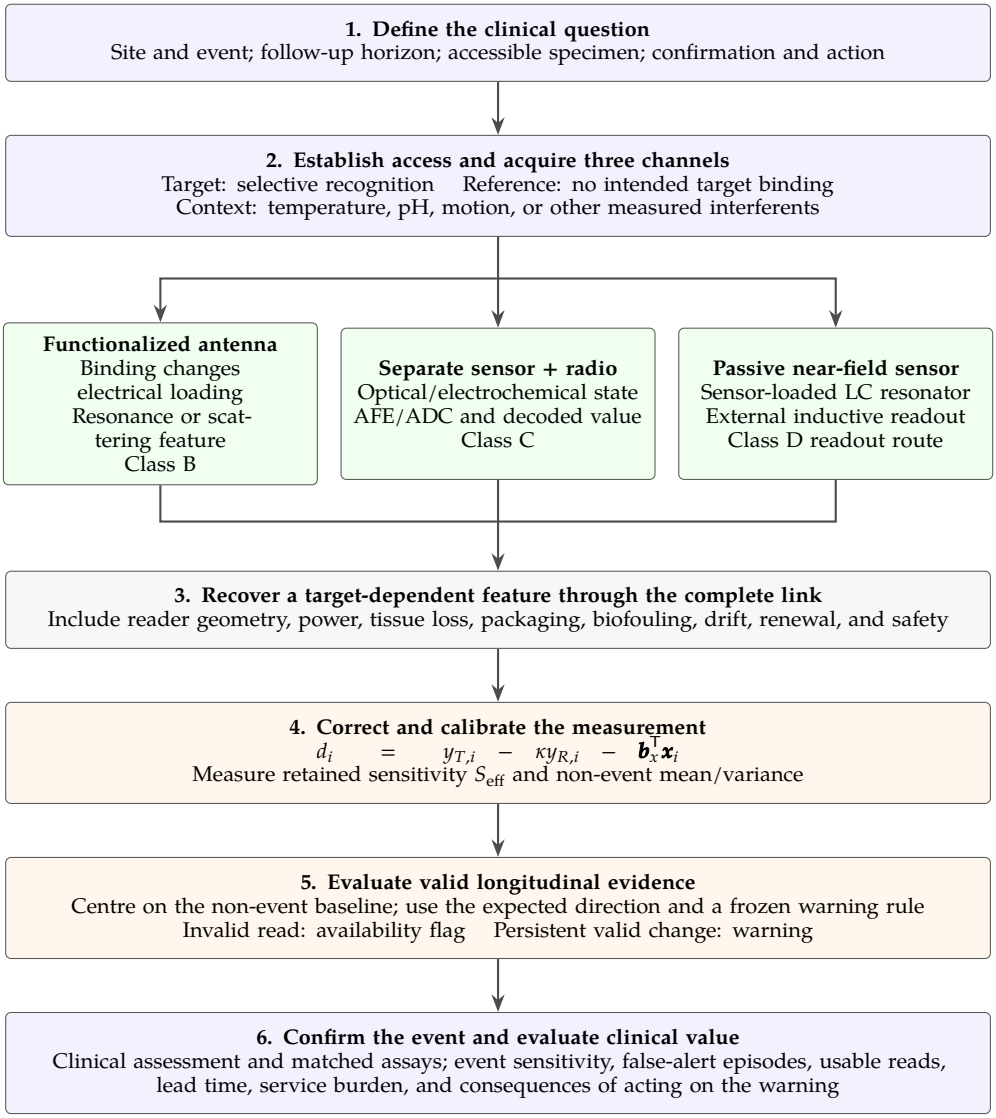


Figure 3. Proposed target–context–reference architecture. The same clinical question can be implemented through a functionalized antenna, a separate sensor with implanted telemetry, or a passive near-field readout. Each route must preserve target information through correction and external acquisition. AFE: analogue front end; ADC: analogue-to-digital converter; LC: inductance–capacitance. The architecture is a testable proposal; clinical confirmation and utility remain separate validation stages.

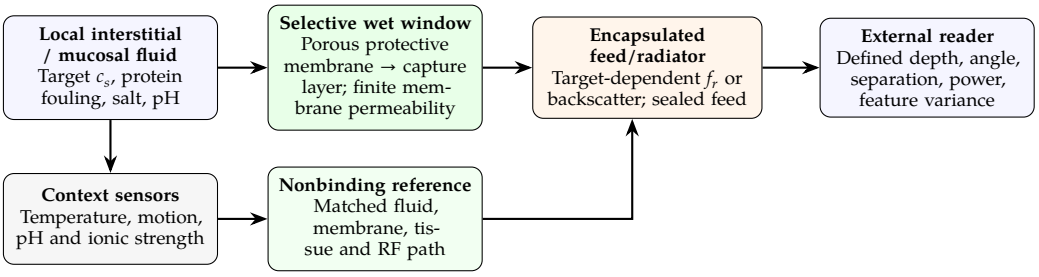


Figure 4. Proposed fluid-facing Class B cross-functional schematic; it is not a fabricated device. The membrane admits the target to the exposed recognition layer while the feed and radio remain sealed. The nonbinding reference experiences a matched matrix/loading path. Both target and benign disturbances must be independently varied while the external reader recovers the feature.

9.2. A Quantitative Requirements Chain

The following model links local sampling, reversible binding, reader observability, and a longitudinal warning. It combines established adsorption, sampling, and detection principles with the reviewed implant evidence [4,7,15,48,60–62]. Its equations are design approximations with stated operating conditions, not a validated universal cancer model. Continuous time is denoted by t and acquisition index by i. All concentrations in the biophysical equations use a consistent molar unit; reported assay ranges in mass units require molecular-mass conversion before molecule counting. Tables 14 and 15 summarize the notation.

Table 14. Biophysical and readout notation. U_c, U_t, U_q, and U_y denote the selected concentration, time, sensor-state, and feature units. The same units are retained within each calibration.

Symbol	Meaning	Units
t; $c_r, c_s, c_{s,0}$	Continuous time; reference, local, and initial local concentration	U_t; U_c
γ_s; r_{loc}	Transfer/recovery coefficient; effective local production rate	1; U_c/U_t
$\mathrm{Da}_s, D, \delta, \Gamma_{\max}$	Surface Damköhler ratio, diffusion coefficient, diffusion-layer thickness, and binding-site density	1; m^2/s; m; $\mathrm{mol}/\mathrm{m}^2$
$\tau_s, \tau_b, \tau_{\mathrm{off}}$	Transport, binding relaxation, and dissociation time constants	U_t
$\theta, \theta_0, \theta_{\mathrm{eq}}$; K_D	Current, initial, and equilibrium occupancy; dissociation constant	1; U_c
$k_{\mathrm{on}}, k_{\mathrm{off}}$	Association and dissociation rate constants	$U_c^{-1}U_t^{-1}$; U_t^{-1}
$N_{\mathrm{cap}}, \lambda$; η_{cap}	Captured count and expected count; capture efficiency	1
V; N_A	Effective sampled volume; Avogadro constant	L; mol^{-1} (with c_s in mol/L)
q_{sensor}; y	Scalar sensor state; real reader feature	U_q; U_y
$S_{\mathrm{bio}}, S_{\mathrm{read}}$	Biochemical and state-to-feature slopes at operating point 0	U_q/U_c; U_y/U_q
$S_{\mathrm{raw}}, S_{\mathrm{eff}}$	Raw-channel and corrected-output concentration slopes	U_y/U_c
$\boldsymbol{\xi}, \boldsymbol{b}$; ϵ	Nuisance vector, its response coefficients; residual error	Per-component units; U_y for error
$y_{T,i}, y_{R,i}, d_i$	Target feature, reference feature, corrected residual	U_y
κ; $\boldsymbol{x}_i, \boldsymbol{b}_x$	Reference coefficient; context vector and coefficients	1; x_j and U_y/x_j per component
a, m; c_*, c_0	Log-calibration intercept/slope; reference/operating concentration	U_y; U_c

Table 15. Decision and coverage notation. Conditional probabilities are defined in the text; all times use a declared common origin.

Symbol	Meaning	Units
i; H_0	Acquisition index; defined non-event condition	Index; condition
$\mu_{d,0}, \sigma_{d,0}$	Non-event residual mean and standard deviation	U_y
σ_{stat}; n_0, n_1	Comparison-statistic standard deviation; baseline/follow-up sample counts	U_y; counts
$\sigma_{\mathrm{stat,corr}}, \sigma_{\mathrm{stat,raw}}$	Corrected and raw comparison-statistic standard deviations	U_y
$\alpha, \beta_{\mathrm{miss}}$; z_p	Per-comparison false-positive/false-negative probability; normal quantile	1

Table 15. *Cont.*

Symbol	Meaning	Units
$\Delta c_{\min}$	Local concentration-change requirement at stated power	U_c
$H; K, k, p_k$	Follow-up horizon; event category, index, and conditional weight	U_t; category/index; 1
$A_k, S_k, R_k; S_{\text{system}}$	Sequential access, detection, delivery probabilities; overall target-mediated sensitivity	1
$T_{\text{release}}, \cdots, T_{\text{decision}}$	Component durations in Equation (8)	U_t
$T_{\text{warning}}, T_{\text{clinical}}, L$	Warning and clinical confirmation times; their lead-time difference	U_t
$N_{\text{read}}, P_{\geq 1\,\text{false}}$	Valid-read count; probability of one or more false-positive reads	Count; 1
s, v_i, r_i, G_i	Response direction, valid-read indicator, standardized residual, CUSUM statistic	1
ν, h, W_i	Reference value, control limit, warning-condition indicator	1
$t_i, t_{\text{last}}, a_i, T_{\text{gap}}$	Acquisition and previous-valid times, elapsed age, maximum permitted gap	U_t
$\widetilde{G}_{i-1}$	Previous statistic after applying the gap-reset rule	1
σ, ρ	Equal channel-noise standard deviation and correlation in the example	U_y; 1
$\sigma_{\text{align}}, \sigma_{\text{load}}$	Assumed residual between-session reader pose and tissue-loading variation	U_y

9.2.1. Step 1: Local Access, Binding, and Molecule Sampling

Let $c_r(t)$ denote concentration in the clinically validated reference specimen and $c_s(t)$ the local fluid concentration immediately adjacent to the sensing surface. One possible lumped transport model is

$$\frac{dc_s}{dt} = \frac{\gamma_s c_r(t) - c_s(t)}{\tau_s} + r_{\text{loc}}(t), \qquad c_s(0) = c_{s,0}. \tag{1}$$

Here, $\gamma_s \geq 0$ is a dimensionless transfer/recovery coefficient, $\tau_s > 0$ is a transport time constant, r_{loc} is an effective local production rate in concentration/time, and $c_{s,0}$ is the initial concentration. The time constant describes gradual equilibration, not a pure travel delay. Equation (1) assumes that the fluid adjacent to the receptor is approximately well mixed and sensor uptake does not appreciably deplete it. An elementary transport-versus-reaction check is $\text{Da}_s = k_{\text{on}}\Gamma_{\max}\delta/D$, with k_{on} expressed in $\text{m}^3\ \text{mol}^{-1}\ \text{s}^{-1}$, surface-site density $\Gamma_{\max}$ in $\text{mol}\ \text{m}^{-2}$, diffusion-layer thickness δ in m, and diffusivity D in $\text{m}^2\ \text{s}^{-1}$. For $\text{Da}_s \ll 1$, replenishment is fast compared with surface uptake; for $\text{Da}_s \gtrsim 1$, a depleted boundary layer can make reaction-limited Langmuir kinetics misleading. Poor perfusion, fibrotic encapsulation, or a thick selective membrane can increase δ or lower effective D. In that regime solve diffusion through the local tissue/membrane coupled to the surface binding flux and measure concentration at the surface, not merely in bulk fluid [49,60]. The coefficient is an empirical concentration-transfer parameter, not an access probability, and need not be bounded by one. Biofilm, fibrosis, and altered perfusion can change both transfer and equilibration [63,64]. Paired longitudinal specimens can constrain the model, but cannot identify γ_s, τ_s, and an arbitrary local source simultaneously; the source must be independently constrained or the mapping treated as empirical. If transfer and local production vanish, c_s decays towards zero after the initial transient.

For a reaction-limited surface with equivalent, independent, reversible binding sites,

$$\begin{aligned} \frac{\mathrm{d}\theta}{\mathrm{d}t} &= k_{\mathrm{on}} c_s (1-\theta) - k_{\mathrm{off}}\theta, \\ \theta_{\mathrm{eq}} &= \frac{c_s}{K_D + c_s}, \qquad K_D = \frac{k_{\mathrm{off}}}{k_{\mathrm{on}}}, \\ \tau_b &= \frac{1}{k_{\mathrm{on}} c_s + k_{\mathrm{off}}}, \qquad \tau_{\mathrm{off}} = \frac{1}{k_{\mathrm{off}}}. \end{aligned} \tag{2}$$

The occupied fraction θ lies between zero and one; an initial occupancy $\theta(0) = \theta_0 \in [0,1]$ completes the dynamic specification. The association rate constant k_{on} has units $U_c^{-1}U_t^{-1}$, and the dissociation rate constant $k_{\mathrm{off}} > 0$ has units U_t^{-1}, where U_c and U_t are the selected concentration and time units; K_D therefore has concentration units. The equilibrium and relaxation expressions assume constant c_s; τ_{off} describes release into target-free fluid. Langmuir-type equilibrium [48] explains loss of concentration sensitivity near saturation. Specifically, $\partial\theta_{\mathrm{eq}}/\partial c_s = K_D/(K_D + c_s)^2$; at $c_s = 10K_D$, the occupancy slope is only $4/121 \approx 3.3\%$ of its value at $c_s = K_D$. Equation (6) therefore uses a local slope at a declared baseline concentration, not a fixed sensitivity across the assay range. Near saturation, increasing sample volume or RF gain cannot restore the lost recognition slope; select an appropriate K_D, a second affinity range, or a renewable window and test both rising and falling concentrations. Slow dissociation also delays recovery after a previous high exposure. Transport-limited, heterogeneous, or irreversible binding needs a different calibration or renewal model; a single binding experiment cannot establish chronic tracking [4,7].

For rare targets, a simple independent-capture model gives

$$\begin{aligned} N_{\mathrm{cap}} &\sim \mathrm{Poisson}(\lambda), \qquad \lambda = \eta_{\mathrm{cap}} c_s V N_A, \\ \Pr(N_{\mathrm{cap}} \geq 1) &= 1 - e^{-\lambda}. \end{aligned} \tag{3}$$

N_{cap} is the captured-molecule count, $0 \leq \eta_{\mathrm{cap}} \leq 1$ the capture efficiency, V the effectively sampled fluid volume over a declared acquisition interval, and N_A the Avogadro constant. For c_s in mol/L and V in L, λ is dimensionless. The well-mixed approximation uses a representative constant local concentration and does not count repeated exposure to the same molecules as new independent sampling. A 95% probability of capturing at least one molecule requires $\lambda \geq -\ln(0.05) = 2.996$. This necessary sampling condition does not establish molecular identity, assay selectivity, or clinical sensitivity [60].

9.2.2. Step 2: A Calibrated Reader Feature and Its Corrected Sensitivity

Let q_{sensor} be a scalar sensor state, such as film conductivity or optical intensity, and let y be a real-valued reader feature, such as resonance frequency, scattering amplitude, phase, or a decoded sensor value. Around a fixed operating point,

$$\begin{aligned} \Delta y &\approx S_{\mathrm{raw}} \Delta c_s + \boldsymbol{b}^{\mathsf{T}} \Delta \boldsymbol{\xi} + \epsilon, \\ S_{\mathrm{raw}} &= \underbrace{\left.\frac{\partial y}{\partial q_{\mathrm{sensor}}}\right|_0}_{S_{\mathrm{read}}} \underbrace{\left.\frac{\partial q_{\mathrm{sensor}}}{\partial c_s}\right|_0}_{S_{\mathrm{bio}}}. \end{aligned} \tag{4}$$

S_{bio} is the biochemical calibration slope, S_{read} the state-to-feature transfer slope, and S_{raw} their product. The subscript 0 denotes the declared operating point. The nuisance vector $\boldsymbol{\xi}$ includes temperature, fluid geometry, motion, nonspecific adsorption, and reader alignment; $\boldsymbol{b}$ gives the corresponding feature-response coefficients. The additive error ϵ has the same units as y. The relation is quasi-static: if transport or binding has not equilibrated, the preceding dynamic model or an explicitly dynamic calibration is needed. Complex impedance or scattering requires a real feature extraction or a vector/Jacobian extension.

For a direct antenna sensor, S_{read} includes the circuit, tissue, and external reader response. For digitized Class-C telemetry, it is the sensor-to-decoded-value calibration; the RF carrier need not change with concentration, and successful packet delivery is a separate availability condition. An electromagnetic load sweep alone determines neither biochemical sensitivity nor recurrence probability.

Acquire the target feature $y_{T,i}$, a nonrecognizing reference feature $y_{R,i}$ in the same units, and measured context vector $\boldsymbol{x}_i$. Define

$$\begin{aligned} d_i &= y_{T,i} - \kappa y_{R,i} - \boldsymbol{b}_x^{\top}\boldsymbol{x}_i, \\ \mu_{d,0} &= \mathrm{E}(d_i \mid H_0), \qquad \sigma_{d,0}^2 = \mathrm{Var}(d_i \mid H_0), \\ S_{\text{eff}} &= \left.\frac{\partial \mathrm{E}(d_i)}{\partial c_s}\right|_0 . \end{aligned} \tag{5}$$

κ is the dimensionless reference-matching coefficient; $\boldsymbol{b}_x$ contains coefficients with units U_y/x_j for context component x_j, where U_y is the feature unit. The condition H_0 means absence of the specified event in the defined monitoring state; $\mu_{d,0}$ and $\sigma_{d,0} > 0$ are its residual mean and standard deviation. Estimate these quantities using independent, representative non-event trajectories, including expected healing and benign disturbances. The variance definition retains context variability and cross-channel covariance rather than assuming independent correction errors. Calibration coefficients are fitted in development and frozen before outcome evaluation [61].

A non-event reference state is not automatically the patient's first postoperative reading. Residual disease may already be present at initialization, and absence of clinically confirmed recurrence does not establish molecular clearance. A rule that tracks change from an already abnormal personal baseline may miss persistent disease. Applications addressing molecular residual disease therefore require an independently validated absolute criterion or a complementary assay. The constant $\mu_{d,0}$ and $\sigma_{d,0}$ used below apply to a predefined monitoring state with sufficiently stable corrected residuals. Monitoring should begin after an explicitly defined stabilization period, or a separately validated model must account for expected postoperative changes. Pooling healing trajectories alone does not establish stationarity. Patient-specific calibration and any re-baselining must follow predefined clinical criteria that prevent a persistent disease-related signal from being absorbed into the reference state.

The effective sensitivity S_{eff} belongs to the corrected output. It equals S_{raw} only when reference and context subtraction preserve the target response. Residual target binding in the reference or disease-responsive context channels can remove useful signal; this must be tested with target and nuisance challenges. A reference therefore requires a demonstrated net benefit, not merely an additional channel.

For one predeclared, direction-oriented Gaussian comparison with equal noise variance under the null and local alternative,

$$\Delta c_{\min} \approx \frac{\left(z_{1-\alpha} + z_{1-\beta_{\text{miss}}}\right)\sigma_{\text{stat}}}{|S_{\text{eff}}|}. \tag{6}$$

This expression requires $S_{\text{eff}} \neq 0$; vanishing corrected sensitivity provides no finite concentration resolution under the local model. Here, α is the false-positive probability for that comparison, β_{miss} the false-negative probability at the declared change, $z_p = \Phi^{-1}(p)$ the standard-normal quantile, and σ_{stat} the standard deviation of the actual comparison statistic. For a single corrected reading against a known baseline mean, $\sigma_{\text{stat}} = \sigma_{d,0}$. For independent baseline and follow-up averages with n_0 and n_1 readings of equal variance,

$$\sigma_{\text{stat}} = \sigma_{d,0}\sqrt{1/n_0 + 1/n_1}.$$

Temporal dependence requires the variance of the correlated comparison, not this independent-read formula. A two-sided comparison uses $z_{1-\alpha/2}$ and its corresponding power calculation. When baseline, slope, or correction parameters are estimated, their uncertainty must be included in predictive uncertainty or assessed using independent calibration and validation data. The expression is a local design requirement, not a clinical LOD or an operating threshold for repeated surveillance.

For the same acquisition design, false-positive probability, and power, reference correction improves local resolution when

$$\frac{|S_{\mathrm{eff}}|}{\sigma_{\mathrm{stat,corr}}} > \frac{|S_{\mathrm{raw}}|}{\sigma_{\mathrm{stat,raw}}}.$$

Here, $\sigma_{\mathrm{stat,corr}} > 0$ and $\sigma_{\mathrm{stat,raw}} > 0$ are the standard deviations of the corrected and raw comparison statistics, respectively, in the same feature units. Reduced variance alone is insufficient if correction removes too much target response.

Logarithmic calibration also changes the slope. If $y = a + m\log_{10}(c_s/c_*)$, where a is a feature intercept, m is the feature change per concentration decade, and $c_* > 0$ is a reference concentration, then the local linear slope at $c_0 > 0$ is $m/(c_0 \ln 10)$. A MHz/decade slope, including the CEA value reported in [4], cannot be used directly as MHz/(ng/mL) in Equation (6). Blank calibration and inverse prediction remain necessary for an analytical LOD.

Illustrative Worked Example

Consider two frequency channels with equal residual noise standard deviation $\sigma = 0.10$ MHz and correlation $\rho = 0.80$, with $\kappa = 1$ and no additional context or model uncertainty. Then, $\sigma_{d,0} = \sigma\sqrt{2(1-\rho)} = 0.0632$ MHz. For an assumed corrected slope of $|S_{\mathrm{eff}}| = 0.50$ MHz/(ng/mL), a single known-baseline comparison with $\alpha = 0.01$ and $1 - \beta_{\mathrm{miss}} = 0.80$ requires approximately $(2.326 + 0.842)0.0632/0.50 = 0.401$ ng/mL. This is a mass-unit calibration example, not a molecule-count calculation. The values are illustrative and do not describe the cited CEA device or any clinical recurrence threshold. They show how correction noise and retained target sensitivity must be considered together.

To make the covariance assumption reproducible, the 0.10 MHz terms in the preceding calculation represent equal target- and reference-channel within-session feature errors, with $\mathrm{Cov}(y_T, y_R) = \rho\sigma^2 = 0.008$ MHz^2 and $\rho = 0.80$. The cited CEA paper supplies a wired 0.01–100 ng/mL calibration range and approximately 2.46 MHz per decade slope, not those noise/correlation values. At an assumed operating point $c_0 = 1$ ng/mL, its reported logarithmic wired slope would correspond to $2.46/(c_0 \ln 10) \approx 1.07$ MHz/(ng/mL) locally; neither the reference-corrected slope nor a body-to-reader slope was measured. The hypothetical 0.50 slope in the example is a design scenario, not a reading from that paper.

Table 16 summarizes the reported values, assumed inputs, and unmeasured quantities used in this feasibility calculation.

Let an illustrative wet, packaged reader introduce independent between-session standard deviations $\sigma_{\mathrm{align}} = 0.12$ MHz and $\sigma_{\mathrm{load}} = 0.15$ MHz after reference correction. Assuming independent Gaussian errors only for this calculation, the total single-read deviation is $\sqrt{0.0632^2 + 0.12^2 + 0.15^2} = 0.202$ MHz. A proposed 0.50 ng/mL change would need $\sigma_{\mathrm{stat}} \leq 0.50(0.50)/(2.326 + 0.842) = 0.079$ MHz at 80% power and 1% per-comparison false-positive risk. The assumed reader therefore fails G3 for that illustrative change: $\Delta c_{\mathrm{min}} \approx 1.28$ ng/mL, or 2.14 ng/mL if correction reduces $|S_{\mathrm{eff}}|$ from 0.50 to 0.30 MHz/(ng/mL). Even ten repeated readings do not repair stable session-to-session alignment/load variation: treating only electronics noise as independent yields $\sigma_{\mathrm{stat}} \approx \sqrt{0.0632^2/10 + 0.12^2 + 0.15^2} = 0.193$ MHz. These assumed magnitudes are sensitivity probes, not literature-derived uncertainty estimates, in-body performance or clinical decision thresholds.

These are first-order bounds around the declared operating concentration. When a predicted concentration change is not small relative to that concentration, inverse nonlinear calibration is required instead of extrapolation of the local slope.

Table 16. Traceability of the CEA feasibility calculation. The range and log slope are reported in [4]; all other numeric inputs are explicitly assumed. "Unknown" means that the source does not demonstrate the required reader experiment.

Input	Value and Evidence Type	Decision Implication
Cabled CEA response [4]	0.01–100 ng/mL; 2.46 MHz/decade, measured	Laboratory calibration; no reader-level S_{eff}
Channel noise/correlation	0.10 MHz each; $\rho = 0.80$, assumed	Corrected within-session noise 0.0632 MHz
Alignment/loading variation	0.12/0.15 MHz, assumed	Reader total 0.202 MHz; measure through final package
Effective slope and target change	0.50 or 0.30 MHz/(ng/mL); 0.50 ng/mL, assumed	Illustrative G3 feasibility boundary only
Untethered reader power, depth, corrected slope, drift	Not established; reported SAR is a simulation	Retain the published exposure result, then measure y_T, y_R in crossed target, confounder, geometry and power challenges

9.2.3. Step 3: Anatomical Coverage, Latency, and Repeated Warnings

Define a follow-up horizon H and a set of eligible surveillance events. Let K identify mutually exclusive event categories; simultaneous local/distant disease requires a mixed category or a prespecified first-event hierarchy. For event-mediated detection,

$$S_{\text{system}} = \sum_k p_k A_k S_k R_k, \qquad \sum_k p_k = 1. \tag{7}$$

Here, $p_k = \Pr(K = k \mid \text{eligible event within } H)$, A_k is the probability of sufficient target access conditional on category k, S_k is correct sensor-detection probability conditional on access and category, and R_k is timely usable-delivery probability conditional on the preceding success conditions. These sequential conditional definitions require no independence assumption. The model describes target-mediated detection; observed clinical sensitivity additionally requires blinded event-window adjudication. Second primaries can be included as a distinct eligible endpoint but are not recurrent disease. A better radio link can improve R_k without creating access to a remote lesion. Tumour-informed assays may also miss genetically distinct second primaries, as observed in the HNSCC cohort [43].

An approximate sequential latency budget is

$$\begin{aligned} T_{\text{warning}} \approx{}& T_{\text{release}} + T_{\text{transport}} + T_{\text{binding}} \\ &+ T_{\text{read}} + T_{\text{decision}}, \\ L ={}& T_{\text{clinical}} - T_{\text{warning}}. \end{aligned} \tag{8}$$

The component durations represent release to a detectable source level, transport, sensor response to its threshold, waiting/acquisition/delivery of a valid read, and the persistence/decision requirement. T_{clinical} is conventional confirmation time and T_{warning} warning time, both measured from the same declared biological or follow-up origin. A positive L is earlier warning. Overlapping processes need a dynamic or empirical timing analysis rather than literal addition; τ_s and τ_b are not automatically threshold-crossing delays. Lead time must be reported with missed events, false alerts, and follow-up censoring and does not alone establish improved outcome.

For N_{read} independent, valid non-event reads with constant per-read false-positive probability α,

$$P_{\geq 1\,\text{false}} = 1 - (1-\alpha)^{N_{\text{read}}}. \tag{9}$$

This is the probability of at least one positive read, not the number of false-alert episodes per patient-year. Dependence can change that probability in either direction; drift can also change the marginal α and generate persistent excursions. Episode burden therefore requires calibration of the complete longitudinal policy.

A direction-aware, quality-gated cumulative-sum (CUSUM) rule [62] is

$$\begin{aligned} r_i &= s\frac{d_i - \mu_{d,0}}{\sigma_{d,0}} \quad \text{for } v_i = 1, \qquad s \in \{-1, +1\}, \\ \widetilde{G}_{i-1} &= G_{i-1}\mathbf{1}\{a_i \leq T_{\text{gap}}\}, \\ G_i &= \begin{cases} \max(0, \widetilde{G}_{i-1} + r_i - \nu), & v_i = 1, \\ \widetilde{G}_{i-1}, & v_i = 0, \end{cases} \qquad G_0 = 0, \\ W_i &= \mathbf{1}\{v_i = 1,\ G_i > h\}. \end{aligned} \tag{10}$$

The valid-read indicator is $v_i \in \{0, 1\}$; r_i is evaluated only for valid reads, and s is fixed so the expected target change increases it. At acquisition time t_i, let $a_i = t_i - t_{\text{last}}$ be elapsed time since the previous valid read (or initialization before the first read), and let $T_{\text{gap}} > 0$ be the maximum permitted gap. The intermediate statistic $\widetilde{G}_{i-1}$ clears stale evidence before processing a new reading, including the first valid reading after a long outage. The dimensionless reference value $\nu > 0$ sets the shift of interest, $h > 0$ is the control limit, and $\mathbf{1}\{\cdot\}$ equals one when its condition holds. W_i denotes an active warning condition. A warning episode begins at its first threshold crossing; repeated positive reads within that episode are not separate alerts. Select ν during development and calibrate h on independent non-event trajectories for the intended false-alert burden, then freeze the policy. Both directions, if required, need joint false-alert calibration.

The gap threshold, post-alert reset, confirmation pathway, refractory interval, and any re-baselining procedure must be specified before validation. A reset is not evidence that cancer is absent; an outdated or invalid calibration keeps $v_i = 0$ until service or recalibration. Invalid reads produce an availability/service flag, never a negative cancer test. Report calendar-time performance and usable-read fraction so missing acquisitions cannot conceal a lost warning window.

For an illustrative half-open 48 h event window $[0, 48)$ h, schedule one read every 6 h at $t_i = 0, 6, \ldots, 42$ h. Suppose each valid event read has standardized residual $r_i = 1$, with $\nu = 0.5$, $h = 1.25$, and $T_{\text{gap}} = 12$ h. Three consecutive valid reads contribute $0.5 + 0.5 + 0.5 = 1.5 > h$. In schedule A, the six valid reads occur at 0, 6, 12, 18, 24 and 30 h, yielding a first warning at 12 h. In schedule B, the six valid reads occur at 0, 6, 24, 30, 36 and 42 h: the 18 h interval between 6 and 24 h resets the statistic, and the first warning occurs at 36 h. Both schedules achieve $6/8 = 75\%$ overall availability, but within $[0, 24)$ h, comprising the scheduled reads at 0, 6, 12 and 18 h but not at 24 h, their event-window usable fractions are $4/4$ and $2/4$, respectively; only A warns within that window. For daily reads at 0, 24 and 48 h with the same residual and decision settings, the first possible warning occurs at 48 h only if $T_{\text{gap}} \geq 24$ h (e.g., 24 h); this is an acquisition-time lower bound, and its third read falls outside $[0, 48)$ h. Retaining $T_{\text{gap}} = 12$ h for daily sampling instead resets G_i before every new read, so the three-read warning cannot occur. The gap limit must therefore be prespecified for each acquisition schedule and the longest outage it permits. Here, each active episode causes a confirmatory assessment, then a prespecified 24 h refractory interval followed by a reset to zero; no alert is counted again until the interval expires, and re-baselining is prohibited without clinical review. None of these numeric settings is a clinical threshold.

Table 17 compares the two six-hour acquisition schedules.

Table 17. Illustrative acquisition example for Equation (10); time 0 is assumed to be the beginning of a detectable local event, not a measured cancer-onset time. Both six-hour schedules have 75% whole-window valid reads. The first-day column counts reads in $[0, 24)$ h, excluding the acquisition at 24 h. The illustrated 12 h gap limit applies to these six-hour schedules, not unchanged to daily acquisition.

Schedule	Valid Read Times, Hours	First Warning	Valid in $[0, 24)$ h
A: late outages	0, 6, 12, 18, 24, 30	12 h	4 of 4
B: early cluster	0, 6, 24, 30, 36, 42	36 h (gap reset)	2 of 4

Accordingly, R_k in Equation (7) must be estimated as the event-conditional probability of receiving enough timely, valid evidence under the actual schedule, reader-use behaviour and outage structure, not from overall packet-success percentage. The deterministic toy residual above ignores correlated biological noise. For a real implant, estimate lagged covariance and baseline trends in non-event trajectories that include healing and sensor ageing; use patient-level time-block resampling, a calibrated state-space/AR noise model, or a prespecified time-dependent baseline that is frozen before independent event validation. Re-estimating a baseline during a suspected event risks absorbing the event. Choose h against complete trajectory simulations and withheld non-event patients to target false-alert episodes per patient-year, then test sensitivity and warning delay with clustered missing reads.

Alert Adjudication and Follow-Up

The follow-up horizon H and the alert-to-event matching window serve different purposes. Before validation, define the eligible event, its independent clinical reference standard, and the interval in which an episode onset can be linked to subsequent event confirmation. Match episodes and events using a fixed rule: the first qualifying episode supplies lead time, and repeated alerts for that event do not create additional true-positive events. Alerts after conventional confirmation are reported separately as late detections. An unmatched episode is classified as false only after adequate subsequent observation; insufficient follow-up leaves its classification indeterminate. For a first-event analysis, at-risk follow-up runs from monitoring entry to the first eligible event, death, withdrawal, or study end. Report false-alert episodes per patient-year over this prespecified at-risk time, indeterminate episodes, and usable-read fraction separately. Death and loss to follow-up require explicit handling; missed acquisitions remain part of calendar follow-up and availability reporting. The numerical matching window and confirmation pathway must be chosen for the indication rather than inferred from the observed results.

Table 18 summarizes limiting conditions. Operational outcomes are event sensitivity by anatomical category, false-alert episodes per patient-year, usable-read fraction, warning lead-time distribution, service interventions, and unnecessary confirmatory procedures. Decision-curve analysis can assess decision value for a defined action, endpoint, and time horizon [65]. Its threshold must represent the clinical trade-off for that action; a CUSUM control limit is not itself a calibrated recurrence probability. Improved analytical sensitivity alone does not establish clinical benefit.

Table 18. Illustrative calculations and limiting conditions. These are design examples, not measured device or clinical results.

Declared Condition	Result	Interpretation
$\gamma_s = 0$, $r_{\mathrm{loc}} = 0$, after equilibration	$c_s \to 0$	An inaccessible target cannot be recovered by improving the antenna.
$c_s \gg K_D$	$\theta_{\mathrm{eq}} \approx 1$	Saturation reduces response to further concentration changes.
Equal independent channel noise; $\kappa = 1$; no extra uncertainty	$\sigma_{d,0} = \sqrt{2}\sigma$	Reference subtraction adds noise unless correlated drift is removed.
Equal channel noise; $\rho = 0.8$; $\kappa = 1$; no extra uncertainty	$\sigma_{d,0} = 0.632\sigma$	Correlated error removal can help if target sensitivity is retained.
365 independent daily reads; $\alpha = 0.01$	97.4% with ≥1 false positive	Per-read 99% specificity does not specify a useful annual alert policy.
365 independent daily reads; $\alpha = 0.001$	30.6% with ≥1 false positive	Count warning episodes using the complete persistence/reset policy.
Only local eligible events provide access	$S_{\mathrm{system}} \leq p_{\mathrm{local}}$	Perfect local detection does not provide whole-body coverage.

9.3. Development Workflow and Validation Gates

Figure 5 is the principal practical outcome of the review. The workflow applies the quantitative chain to five decisions: biological access (G1), assay serviceability (G2), complete-link observability (G3), clinical validity (G4), and clinical utility (G5). Passing an engineering gate does not establish clinical benefit. Each gate has three legitimate outcomes: advance when the criterion is met, revise the target/interface when the problem is correctable, or stop when an implanted system offers no advantage over an accessible test. The gates make clear which limitation an RF improvement can address.

The workflow supports a prespecified development protocol. Calibrate target and nuisance responses separately, then test withheld combined challenges to establish whether the target remains distinguishable. Freeze the baseline, features, quality rules, and warning policy before prospective evaluation. A persistent valid warning initiates confirmatory assessment within the defined clinical pathway.

A factorial validation matrix (Table 19) tests whether the reference helps rather than merely removing variation. Each challenge has a matched target-absent and target-present version, with concentrations and reader geometry measured independently. Estimate raw and corrected sensitivity in the same held-out specimens; improvement requires both reduced non-event variation and preservation of target response as formalized below Equation (6). Do not train the correction on the same individual trajectories used to evaluate specificity.

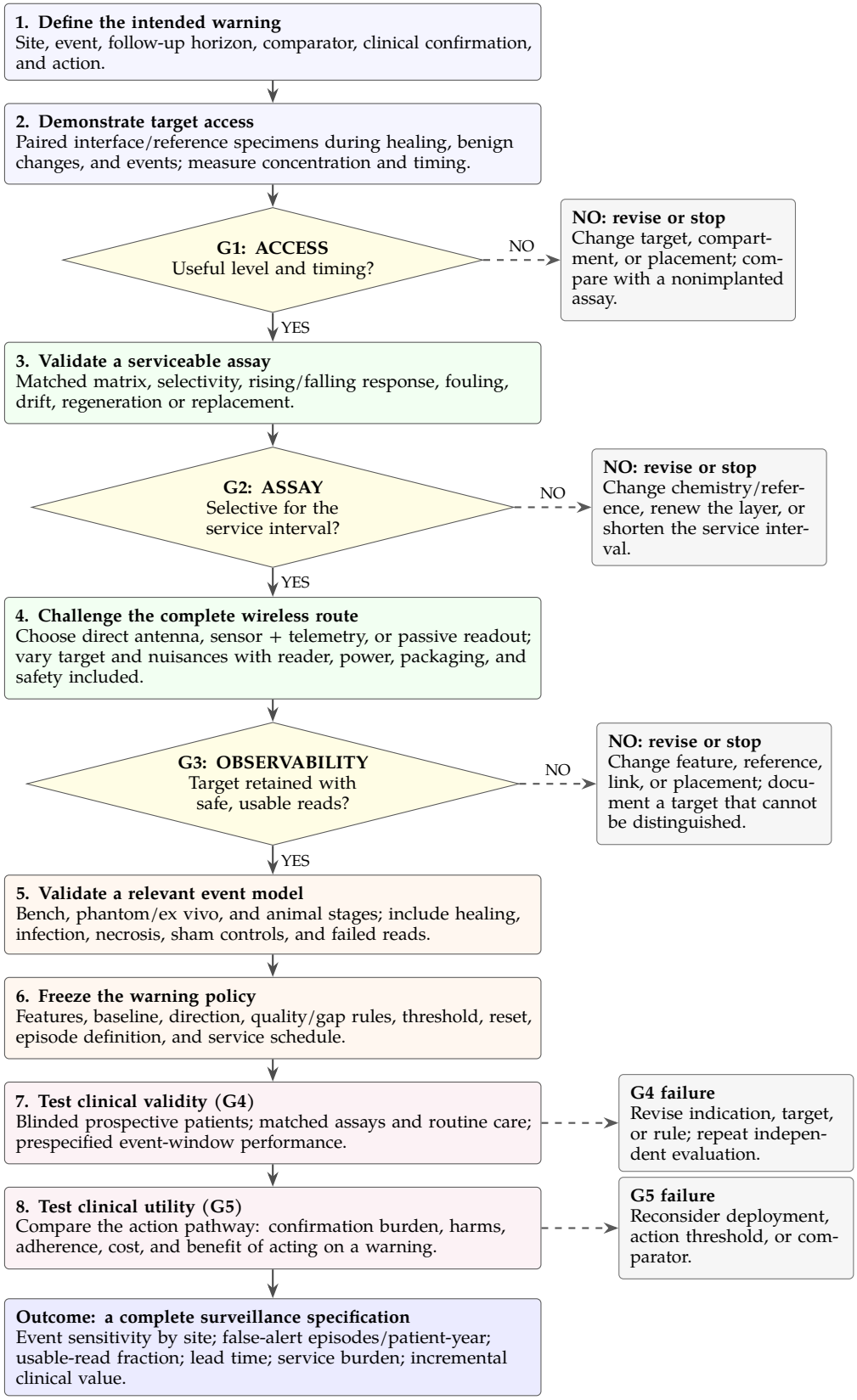


Figure 5. Evidence-to-device workflow. G1–G3 establish biological access, assay serviceability, and complete-link observability. G4 tests clinical validity with a frozen rule; G5 tests the consequences of acting on the warning. Advancement requires the prespecified criterion at each stage. A failed stage prompts revision or stopping, followed by independent evaluation when development resumes.

Table 19. Predeclared challenge matrix for a local cancer interface. Match the target-present and target-absent arms within the relevant anatomy; a target-positive specimen need not itself establish cancer.

Challenge	Matched Contrast and Independent Reference	Acceptance Question
Healing/inflammation	Postoperative time and inflammatory markers with biopsy-negative follow-up	Does corrected false-alert burden fall without losing tumour-associated response?
Infection/treatment effect	Culture/clinical infection or mucositis, therapy stage, matched tumour-negative controls	Are responses identifiable before and after therapy, at constant target level?
Fibrosis/biofouling	Interface histology, membrane permeability, repeated wet exposures	Is access, S_{eff}, and valid-read fraction preserved through service life?
Reader pose/ionic loading	Crossed displacement, polarization, depth and salt changes at fixed analyte	Does the reader retain target discrimination with final packaging and safe power?
Drift/second primary	Age-matched blanks; independent event genotyping and adjudication	Are drift excursions counted, and is second-primary coverage reported separately?

Table 20 translates the workflow into measurable examples without imposing a universal performance standard. The numerical values illustrate one possible study protocol and must be replaced by indication-specific targets, clinically meaningful event windows, and justified sample sizes before data collection. A "pass" cannot be claimed by measuring only a favourable subset of reads or events.

Table 20. Gate acceptance template. Requirements in the middle column are mandatory to support the corresponding claim; numeric values in the last column are illustrative protocol choices only, not established clinical standards.

Gate	Required Measurement and Fail Condition	Illustrative Target to Prespecify
G1 access	Paired local/reference concentration and lag across event and benign windows; fail if insufficient accessible target	At least 80% of eligible local-event windows above a validated matrix blank
G2 assay	Wet rise/fall target slope, interferents and drift through chosen service interval; fail if correction erases signal	Less than 20% loss of net sensitivity over a declared 30-day service test
G3 link	External-reader S_{eff}, variance, worst-case power/SAR, tissue/orientation and missing reads; fail if target change unresolvable	At least 90% valid reads in each declared 24 h event window, plus power-compliant margin
G4 validity	Frozen rule, blinded reference, all missed reads, site-stratified event and non-event time; fail if false alerts or missed events excessive	At least 80% local-event sensitivity and no more than 0.5 unmatched episodes per patient-year, with CIs
G5 utility	Confirmatory-work-up burden, harm, adherence and comparative net benefit; fail if no action advantage	Positive predeclared decision benefit vs accessible testing and routine care

Applying the Gates to the Published CEA Antenna

The CEA antenna in [4] illustrates how the gates separate a useful transduction result from a surveillance claim (Table 21). Its measured concentration range and frequency response support molecular-to-RF transduction. Prepared and diluted specimens, however, do not establish the local concentration available to a chronic implant. Likewise, a cable/VNA measurement does not determine how precisely the packaged device can recover the same target feature through tissue. Without the wet packaged reader response, nuisance covariance, and corrected sensitivity, Equation (6) cannot supply a device-specific in-body concentration requirement. The immediate experiment is therefore a continuously exposed, matched-matrix sensor tested through the intended reader geometry, with independently

varied CEA and benign disturbances. A positive result would support advancement through G2/G3; it would still require an endpoint-specific G1 study before a local surveillance claim. This ordering preserves the published contribution while identifying the evidence needed for its next use.

Table 21. Application of G1–G5 to the CEA antenna evidence in [4]. "Partial" denotes evidence for one component of a gate; "unestablished" denotes a requirement not established by the cited experiment. These are claim-specific judgments, not a numerical quality score.

Gate/Status	Published Evidence	Next Decisive Test
G1 access: unestablished	CEA assays include prepared solutions and 5%-serum recovery; paired chronic implant-interface concentrations are not established.	Measure CEA at the intended interface during non-event states and defined events.
G2 assay: partial	A 0.01–100 ng/mL response and controlled stability support analytical transduction; the preparation includes washing/drying.	Test continuous wet exposure, interference, rising/falling concentrations, and renewal over the intended service interval.
G3 link: partial	Frequency response is measured using a cable/VNA; CEA-dependent far-field gain and simulated SAR are also reported; untethered through-tissue analyte recovery remains unestablished.	Recover the feature through tissue with final packaging, realistic reader alignment, reference correction, and safe operating power.
G4 validity: unestablished	No prospective patient-level recurrence endpoint is established by the assay.	Evaluate a frozen warning rule with blinded event adjudication and failed reads included.
G5 utility: unestablished	Benefit from acting on an implanted warning is not evaluated.	Compare the complete confirmation/action pathway with an accessible CEA assay and routine follow-up.

9.4. Stage-Specific Validation and Reporting

Table 22 organizes evidence that should accompany progressively stronger claims. A study can make a valuable contribution at an early stage if it states its endpoint accurately. A phantom perturbation study establishes response under controlled loading; an animal recurrence experiment evaluates a defined model event; prospective human studies establish patient-level performance. Keeping these claims distinct makes different groups' results easier to combine.

Chronic-interface claims require particular care. Protein adsorption, immune response, fibrosis, biofilm, and surface chemistry can alter target delivery and electrical response simultaneously. Anti-fibrotic interfaces provide a promising materials direction [64]; glucose microsystems demonstrate complete biochemical-to-wireless integration in another disease [51]. Glucose-oriented implanted antennas and passive sensors offer transferable tissue and RF methods [66–68] but cannot supply cancer selectivity by analogy. The service interval and explant/replacement route belong in the system specification from the outset. RF power transfer and telemetry require frequency-specific exposure assessment, with operating power and duty cycle stated [59]. General exposure guidance does not replace device-specific evaluation of local heating, tissue contact, packaging, and chronic implant safety.

For data-driven interpretation, partition patients or independent biological models before assigning repeated measurements to development and validation sets. Report independent patient, animal, device, event, and specimen counts separately from repeated reads.

Distinguish technical replicates from independent biological replication, and estimate confidence intervals with this dependence respected. Measure false alerts per patient-year, including those caused by healing or sensor drift; report reader failures and service needs rather than discarding them as unusable data. A study with excellent accuracy on a favourable laboratory dataset can fail operationally when these burdens are counted.

Table 22. Validation gates and the strongest claim supported at each stage. Each claim is limited by the experimental setting, controls, and endpoint evaluated.

Gate	Minimum Evidence	Critical Control	Supported Claim
Biological access (G1)	Paired target levels at device interface and validated specimen	Non-event and benign postoperative samples	The interface samples the chosen target.
Analytical selectivity (G2)	Blinded matched-matrix range, interference, reversibility, drift	Nonbinding surface; nonspecific proteins; pH/ionic changes	The sensor resolves target under stated conditions.
Chronic operation (G2)	Fouling, renewal, materials, repeated exposure/recovery	Reference assay and repeated cycles	Operation for a stated service interval.
Wireless observability (G3)	Reader-included target/nuisance tests, power, availability	Bare antenna; target-only; reference configuration	Target-dependent data are recoverable in the intended geometry.
Preclinical event	Independent event model with blinded adjudication	Healing, infection, necrosis, sham/nonmalignant response	A defined animal-model event is detected.
Clinical validity (G4)	Prospective patients; frozen rule; site-stratified events	Routine surveillance and matched assays	Stated patient-level event performance.
Clinical utility (G5)	Defined action pathway and comparative study	Harms, procedures, adherence, cost	Acting on the warning improves a decision/outcome.

9.5. A Prioritized Research Agenda

Three directions emerge from the evidence. First, functionalized antenna sensing should progress from purified analyte or diluted serum to a matched, continuously exposed biological interface with a reference channel. The decisive result is retention of target information under interference, repeated exposure, and service-related drift. Second, oral/head-and-neck work should begin with endpoint-matched clinical targets, separating OPMD transformation, local recurrence, nodal recurrence, and HPV-associated disease. Third, deep lung and other internal-organ systems should establish biological access and coverage before borrowing a plasma biomarker's performance.

For an initial oral study, this framework leads to a practical specification: define recurrence or OPMD transformation as a separate endpoint; measure the corresponding protein/cytokine targets at the intended oral interface; compare a serviceable target–reference surface with the same target channel alone; and test whether context improves interpretation through inflammation and healing. The primary comparison should use a fixed false-alert-episode burden and a minimum usable-read requirement. A positive result would justify further implanted integration; a negative result would identify whether access, selectivity, renewal, or the wireless route limits the indication. Deep-organ work requires the analogous local-fluid/reference-specimen study before a plasma assay's performance can inform an implant claim.

9.6. Limits of the Synthesis

The source set is heterogeneous, and the targeted narrative search cannot establish an exhaustive census or the absence of relevant work for every organ. Some studies use short animal experiments, prepared fluids, externally supplied probes, or partly conceptual electronics. Clinical biomarker evidence concerns different populations and treatment stages, so no pooled diagnostic accuracy is computed. Related clinical cohorts and device families are not independent replications. The mathematical model is approximate; transport, binding, radio responses, and noise can become nonlinear or time-varying.

The review cannot supply effect sizes for local target access, packaged reader variability, or event-window clinical utility where no appropriate study exists. The gate values in Table 20 are illustrative design choices, not extrapolated estimates. Long-term foreign-body effects, probe replenishment, and diagnostic errors caused by missing reads remain prospective experimental questions.

10. Conclusions

Implantable antennas can support cancer surveillance by sensing local dielectric changes, converting molecular recognition into an RF feature, or transmitting a separate sensor's measurement. Published studies establish these routes at different evidence levels, including animal recurrence monitoring with RF telemetry. The next challenge is a durable measurement pathway that matches a particular event, anatomical compartment, and clinical response.

The evidence map and the CEA case study identify three immediate priorities: establish target access in the intended compartment; preserve target information through chronic exposure and complete wireless readout; and evaluate a frozen warning rule against independently adjudicated events. Baseline validity, alert matching, failed reads, and service interventions are part of that evaluation. Oral and head-and-neck applications offer accessible interfaces, but saliva, mucosal fluid, regional disease, recurrence, and malignant transformation require separate validation. Lung and other deep-organ applications face greater sampling and coverage constraints. Physiological channels can add context, provided their contribution is tested against the target-only measurement.

The outcome of this review is a specification for choosing and evaluating the next experiment. The quantitative chain explains where information can be lost; the five validation gates identify when to advance, revise, or stop. Clinical utility ultimately depends on whether acting on a warning improves the management pathway at an acceptable procedural and false-alert burden.

Funding: This study (under CanDia CUP E13C24002390006) was supported by the European Union—NextGenerationEU, under the Italian National Recovery and Resilience Plan (NRRP), Mission 4 Component 2 Investment 1.2, funding scheme "Young Researchers" (D.D. 201 del 3.7.2024).

Institutional Review Board Statement: Not applicable. This review reports no new studies involving humans or animals.

Informed Consent Statement: Not applicable.

Data Availability Statement: No new datasets were generated. All evidence discussed in this critical narrative review is available in the cited publications.

Conflicts of Interest: The author declares no conflicts of interest.

Abbreviations

The following abbreviations are used in this manuscript:

ADC	Analogue-to-digital converter
AFE	Analogue front end
BLE	Bluetooth low energy
CEA	Carcinoembryonic antigen
CUSUM	Cumulative sum
ctDNA	Circulating tumour DNA
DFS	Disease-free survival
EpCAM	Epithelial cell adhesion molecule
GI	Gastrointestinal
HE4	Human epididymis protein 4
HNSCC	Head-and-neck squamous cell carcinoma
HR	Hazard ratio
LC	Inductor–capacitor
MRD	Molecular residual disease
NSCLC	Non-small-cell lung cancer
OPMD	Oral potentially malignant disorder
OSCC	Oral squamous cell carcinoma
RF	Radiofrequency
ROS	Reactive oxygen species
VNA	Vector network analyser
WPT	Wireless power transfer

References

1. Bray, F.; Laversanne, M.; Sung, H.; Ferlay, J.; Siegel, R.L.; Soerjomataram, I.; Jemal, A. Global cancer statistics 2022: GLOBOCAN estimates of incidence and mortality worldwide for 36 cancers in 185 countries. *CA Cancer J. Clin.* **2024**, *74*, 229–263. [CrossRef] [PubMed]
2. Aguirre-Ghiso, J.A.; Bravo-Cordero, J.J.; Guo, W.; Lauvau, G.; Sosa, M.S. The sleeping threat: Targeting cancer dormancy to transform metastasis therapy. *Nat. Rev. Cancer* **2026**, *26*, 513–533. [CrossRef] [PubMed]
3. Wang, W.; Xuan, X.-W.; Zhao, W.-Y.; Nie, H.-K. An implantable antenna sensor for medical applications. *IEEE Sens. J.* **2021**, *21*, 14035–14042. [CrossRef]
4. Chen, Y.; Xuan, X.; Li, M.; Jiang, D.; Li, H. Implantable antenna immunosensor based on Au-decorated graphene film for wireless CEA detection. *Sens. Actuators B Chem.* **2024**, *416*, 136037. [CrossRef]
5. Kim, K.; Min, I.S.; Kim, T.H.; Kim, D.H.; Hwang, S.; Kang, K.; Kim, K.; Park, S.; Lee, J.; Cho, Y.U.; et al. Fully implantable and battery-free wireless optoelectronic system for modulable cancer therapy and real-time monitoring. *npj Flex. Electron.* **2023**, *7*, 41. [CrossRef]
6. Nie, R.; Jia, Q.; Li, Y.; Yan, C.; Liu, X.; Tao, Y.; Zhang, J.; Li, P.; Huang, W. Implantable biophotonic device for wirelessly cancer real-time monitoring and modulable treatment. *Adv. Sci.* **2025**, *12*, 2503778. [CrossRef] [PubMed]
7. Weng, Y.; Tang, J.; Long, Z.; Mi, Y.; Han, Q.; Fang, Z.; Xing, L.; Shen, H.; Xue, X.; Chen, M. A battery-free wireless implantable biosensor for postoperative breast cancer recurrence monitoring. *Sens. Actuators B Chem.* **2027**, *471*, 141045. [CrossRef]
8. Mohan, A.; Kumar, N. Implantable antennas for biomedical applications: A systematic review. *Biomed. Eng. Online* **2024**, *23*, 87. [CrossRef] [PubMed]
9. Kassanos, P.; Hourdakis, E. Implantable passive sensors for biomedical applications. *Sensors* **2025**, *25*, 133. [CrossRef] [PubMed]
10. Chimene, D.; Queener, K.M.K.; Ko, B.S.; McShane, M.; Daniele, M. Insertable biosensors: Combining implanted sensing materials with wearable monitors. *Annu. Rev. Biomed. Eng.* **2024**, *26*, 197–221. [CrossRef] [PubMed]
11. Montoya-Villada, S.; Reyes-Vera, E.; Orozco, J. Microwave technologies for biomedical diagnosis and therapy: Advances, challenges, and perspectives. *Microchim. Acta* **2026**, *193*, 218. [CrossRef] [PubMed]
12. Bastías, D.; Maturana, A.; Marín, C.; Martínez, R.; Niklander, S.E. Salivary biomarkers for oral cancer detection: An exploratory systematic review. *Int. J. Mol. Sci.* **2024**, *25*, 2634. [CrossRef] [PubMed]
13. Smida, J.; Azizi, M.K.; Bose, A.S.C.; Waly, M.I. A compact implantable multiple-input-multiple-output antenna for biotelemetry and sensing applications. *Sensors* **2025**, *25*, 3323. [CrossRef] [PubMed]
14. Smida, A. Telemetry and sensing using a dual-element implantable MIMO antenna system. *Sensors* **2026**, *26*, 1694. [CrossRef] [PubMed]
15. Daniel, K.D.; Kim, G.Y.; Vassiliou, C.C.; Galindo, M.; Guimaraes, A.R.; Weissleder, R.; Charest, A.; Langer, R.; Cima, M.J. Implantable diagnostic device for cancer monitoring. *Biosens. Bioelectron.* **2009**, *24*, 3252–3257. [CrossRef] [PubMed]

16. Williams, R.M.; Lee, C.; Galassi, T.V.; Harvey, J.D.; Leicher, R.; Sirenko, M.; Dorso, M.A.; Shah, J.; Olvera, N.; Dao, F.; et al. Noninvasive ovarian cancer biomarker detection via an optical nanosensor implant. *Sci. Adv.* **2018**, *4*, eaaq1090. [CrossRef] [PubMed]
17. Li, S.; Lu, D.; Li, S.; Liu, J.; Xu, Y.; Yan, Y.; Zárate Rodriguez, J.; Bai, H.; Avila, R.; Kang, S.; et al. Bioresorbable, wireless, passive sensors for continuous pH measurements and early detection of gastric leakage. *Sci. Adv.* **2024**, *10*, eadj0268. [CrossRef] [PubMed]
18. Mannoor, M.S.; Tao, H.; Clayton, J.D.; Sengupta, A.; Kaplan, D.L.; Naik, R.R.; Verma, N.; Omenetto, F.G.; McAlpine, M.C. Graphene-based wireless bacteria detection on tooth enamel. *Nat. Commun.* **2012**, *3*, 763. [CrossRef] [PubMed]
19. Tseng, P.; Napier, B.; Garbarini, L.; Kaplan, D.L.; Omenetto, F.G. Functional, RF-trilayer sensors for tooth-mounted, wireless monitoring of the oral cavity and food consumption. *Adv. Mater.* **2018**, *30*, 1703257. [CrossRef] [PubMed]
20. Ahmad, M.Y.; Petrović, B.; Putnik, I.; Kojić, S.; Ibrahim, F.; Milić, L.; Alkhalaf, H.Y.; Stojanović, G.M. Flexible loop tunable antenna for optimized LC sensor integration in salivary analyte applications. *IEEE J. Electromagn. RF Microw. Med. Biol.* **2026**, *10*, 386–396. [CrossRef]
21. Franzmann, E.J.; Qi, Y.; Peifer, S.; Messer, K.; Messing, B.; Blanco, R.G.; Khan, Z.; Fahkry, C.; Coffey, C.; Califano, J., III. Salivary CD44 and total protein levels to detect risk for oral and oropharyngeal cancer recurrence: A nonrandomized clinical trial. *JAMA Otolaryngol. Head Neck Surg.* **2024**, *150*, 843–850. [CrossRef] [PubMed]
22. Raslan, S.; Smith, D.H.; Reis, I.M.; Peifer, S.J.; Forman, G.; Ezeh, U.C.; Joshi, P.; Koester, M.; Buitron, I.; Al-Awady, A.; et al. Soluble CD44 in oral rinses for the early detection of cancer: A prospective cohort study in high-risk individuals. *BMC Oral Health* **2024**, *24*, 820. [CrossRef] [PubMed]
23. Abbosh, C.; Frankell, A.M.; Harrison, T.; Kisistok, J.; Garnett, A.; Johnson, L.; Veeriah, S.; Moreau, M.; Chesh, A.; Chaunzwa, T.L.; et al. Tracking early lung cancer metastatic dissemination in TRACERx using ctDNA. *Nature* **2023**, *616*, 553–562. [CrossRef] [PubMed]
24. Schaufler, A.; Sanin, A.Y.; Sandalcioglu, I.E.; Hartmann, K.; Croner, R.S.; Perrakis, A.; Wartmann, T.; Boese, A.; Kahlert, U.D.; Fischer, I. Concept of a fully-implantable system to monitor tumor recurrence. *Sci. Rep.* **2023**, *13*, 16362. [CrossRef] [PubMed]
25. Chen, Y.-W.; Shiah, S.-G.; Yuan, S.-S.; Wang, Y.-Y.; Tsai, F.-Y.; Chen, I.-C.; Lin, C.-M.; Chung, T.-T.; Lee, J.-J.; Chen, M.-K.; et al. A saliva-based surrogate associates with clinical outcome of oral potentially malignant disorders. *Br. J. Cancer* **2026**, *135*, 818–829. [CrossRef] [PubMed]
26. Chera, B.S.; Kumar, S.; Shen, C.; Amdur, R.; Dagan, R.; Green, R.; Goldman, E.; Weiss, J.; Grilley-Olson, J.; Patel, S.; et al. Plasma circulating tumor HPV DNA for the surveillance of cancer recurrence in HPV-associated oropharyngeal cancer. *J. Clin. Oncol.* **2020**, *38*, 1050–1058. Erratum in *J. Clin. Oncol.* **2023**, *41*, 4449. https://doi.org/10.1200/JCO.23.01228. [CrossRef]
27. Earland, N.; Semenkovich, N.P.; Ramirez, R.J.; Gerndt, S.P.; Harris, P.K.; Gu, Z.; Hearn, A.I.; Inkman, M.; Szymanski, J.J.; Whitfield, D.; et al. Sensitive MRD detection from lymphatic fluid after surgery in HPV-associated oropharyngeal cancer. *Clin. Cancer Res.* **2024**, *30*, 1409–1421. [CrossRef] [PubMed]
28. Gale, D.; Heider, K.; Ruiz-Valdepenas, A.; Hackinger, S.; Perry, M.; Marsico, G.; Rundell, V.; Wulff, J.; Sharma, G.; Knock, H.; et al. Residual ctDNA after treatment predicts early relapse in patients with early-stage non-small cell lung cancer. *Ann. Oncol.* **2022**, *33*, 500–510. [CrossRef] [PubMed]
29. Tang, J.; Tian, Y.; Wang, S.; Liu, Y.; Chen, M.; Yang, X.; Tong, X.; Wang, M.; Zhao, Y.; Pang, J.; et al. Early postoperative plasma circulating tumour DNA for molecular residue disease detection and recurrence risk evaluation in surgical non-small cell lung cancer. *Clin. Transl. Med.* **2024**, *14*, e70056. [CrossRef] [PubMed]
30. Kotani, D.; Oki, E.; Nakamura, Y.; Yukami, H.; Mishima, S.; Bando, H.; Shirasu, H.; Yamazaki, K.; Watanabe, J.; Kotaka, M.; et al. Molecular residual disease and efficacy of adjuvant chemotherapy in patients with colorectal cancer. *Nat. Med.* **2023**, *29*, 127–134. [CrossRef] [PubMed]
31. Mo, S.; Zhou, C.; Ma, M.; Luo, W.; Li, Y.; Lu, P.; Tang, P.; Li, Y.; Ma, X.; Hu, X.; et al. Dynamic circulating tumor DNA methylation monitoring guiding postoperative surveillance in nonmetastatic colorectal cancer. *J. Clin. Oncol.* **2026**, *advance online publication*. [CrossRef] [PubMed]
32. Schaner, P.E.; Pettus, J.R.; Flood, A.B.; Williams, B.B.; Jarvis, L.A.; Chen, E.Y.; Pastel, D.A.; Zuurbier, R.A.; diFlorio-Alexander, R.M.; Swartz, H.M.; et al. OxyChip implantation and subsequent electron paramagnetic resonance oximetry in human tumors is safe and feasible: First experience in 24 patients. *Front. Oncol.* **2020**, *10*, 572060. [CrossRef] [PubMed]
33. Zhu, G.-Q.; Liu, W.-R.; Tang, Z.; Qu, W.-F.; Fang, Y.; Jiang, X.-F.; Song, S.-S.; Wang, H.; Tao, C.-Y.; Zhou, P.-Y.; et al. Serial circulating tumor DNA to predict early recurrence in patients with hepatocellular carcinoma: A prospective study. *Mol. Oncol.* **2022**, *16*, 549–561. [CrossRef] [PubMed]
34. Nitschke, C.; Markmann, B.; Walter, P.; Badbaran, A.; Tölle, M.; Kropidlowski, J.; Belloum, Y.; Goetz, M.R.; Bardenhagen, J.; Stern, L.; et al. Peripheral and portal venous KRAS ctDNA detection as independent prognostic markers of early tumor recurrence in pancreatic ductal adenocarcinoma. *Clin. Chem.* **2023**, *69*, 295–307. [CrossRef] [PubMed]

35. Vedeld, H.M.; Pharo, H.; Sørbø, A.K.; Brandt-Winge, S.; Five, M.-B.; Jeanmougin, M.; Guldberg, P.; Wahlqvist, R.; Lind, G.E. Distinct longitudinal patterns of urine tumor DNA in patients undergoing surveillance for bladder cancer. *Mol. Oncol.* **2024**, *18*, 2684–2695. [CrossRef] [PubMed]
36. European Commission Joint Research Centre. 2024 Estimates of Cancer Cases and Deaths in the EU. Factsheet, February 2026. Available online: https://ecis.jrc.ec.europa.eu/sites/default/files/2026-02/2024%20ESTIMATES%20OF%20CANCER%20CASES%20AND%20DEATHS%20IN%20THE%20EU.pdf (accessed on 6 November 2026).
37. Bando, H.; Watanabe, J.; Takahashi, Y.; Kotaka, M.; Matsuhashi, N.; Oki, E.; Komatsu, Y.; Shiozawa, M.; Hirata, K.; Miyamoto, Y.; et al. Post-adjuvant chemotherapy in ctDNA-positive patients with resected colorectal cancer: A randomized phase 3 trial. *Nat. Med.* **2026**, *32*, 2473–2480. [CrossRef] [PubMed]
38. Kagitha, B.S.N.K.; Ghosh, K.; Das, B.; Goel, V.; Chakraborty, C.; Chakraborty, U. Frequency-reconfigurable dual-polarized implantable antenna for enhanced tumor detection and monitoring via machine learning. *J. Electromagn. Waves Appl.* **2026**, *40*, 1946–1974. [CrossRef]
39. Chen, Z.; Xuan, X.; Li, H.; Dong, X.; Xiao, T.; Jiang, D.; Li, C.; Li, H.; Li, M. Eight-channel vertical-graphene antenna immunosensor array for rapid detection of CYFRA 21-1 in human serum. *Biosens. Bioelectron.* **2026**, *296*, 118329. [CrossRef] [PubMed]
40. Jo, H.J.; Yang, J.-H.; Robby, A.I.; Lee, G.; Jin, E.-J.; Park, S.Y. Cancer microenvironment-recognizable negative–positive electronic signal-based pore size-tunable pH/ROS-responsive hydrogel sensor. *Sens. Actuators B Chem.* **2023**, *390*, 133945. [CrossRef]
41. Corsi, M.; Maurina, E.; Surdo, S.; Vandini, E.; Daini, E.; Vilella, A.; Leo, G.; Farshchian, M.; Grisendi, G.; Golinelli, G.; et al. In vivo and in situ monitoring of doxorubicin pharmacokinetics with an implantable bioresorbable optical sensor. *Sci. Adv.* **2025**, *11*, eads0265. [CrossRef] [PubMed]
42. Chen, L.Y.; Tee, B.C.-K.; Chortos, A.L.; Schwartz, G.; Tse, V.; Lipomi, D.J.; Wong, H.-S.P.; McConnell, M.V.; Bao, Z. Continuous wireless pressure monitoring and mapping with ultra-small passive sensors for health monitoring and critical care. *Nat. Commun.* **2014**, *5*, 5028. [CrossRef] [PubMed]
43. Flach, S.; Pipinikas, C.; Huberty, T.; Lechner, A.; Murray, C.; Marsico, G.; Howarth, K.; Walz, C.; Käsmann, L.; Mock, A.; et al. Personalized ctDNA analysis for detection of residual disease and recurrence in surgically treated HNSCC patients. *npj Precis. Oncol.* **2026**, *10*, 103. [CrossRef] [PubMed]
44. Wei, F.; Patel, P.; Liao, W.; Chaudhry, K.; Zhang, L.; Arellano-Garcia, M.; Hu, S.; Elashoff, D.; Zhou, H.; Shukla, S.; et al. Electrochemical sensor for multiplex biomarkers detection. *Clin. Cancer Res.* **2009**, *15*, 4446–4452. [CrossRef] [PubMed]
45. Torrente-Rodríguez, R.M.; Campuzano, S.; Ruiz-Valdepeñas Montiel, V.; Gamella, M.; Pingarrón, J.M. Electrochemical bioplatforms for the simultaneous determination of interleukin (IL)-8 mRNA and IL-8 protein oral cancer biomarkers in raw saliva. *Biosens. Bioelectron.* **2016**, *77*, 543–548. [CrossRef] [PubMed]
46. Lei, Y.; Zhang, D.; Wang, Q.; Mao, S.; Kim, E.-S.; Kim, N.-Y.; Zhou, Q.; Li, Y.; Yao, Z. Detection of carcinoembryonic antigen specificity using microwave biosensor with machine learning. *Biosens. Bioelectron.* **2025**, *269*, 116908. [CrossRef] [PubMed]
47. Montoya-Villada, S.; Orozco, J.; Reyes-Vera, E. Microwave-based label-free immunosensor to detect anti-p53 autoantibodies. *Sens. Actuators B Chem.* **2025**, *437*, 137702. [CrossRef]
48. Langmuir, I. The adsorption of gases on plane surfaces of glass, mica and platinum. *J. Am. Chem. Soc.* **1918**, *40*, 1361–1403. [CrossRef]
49. Squires, T.M.; Messinger, R.J.; Manalis, S.R. Making it stick: Convection, reaction and diffusion in surface-based biosensors. *Nat. Biotechnol.* **2008**, *26*, 417–426. [CrossRef] [PubMed]
50. Gulati, P.; Singh, A.K.; Yadav, A.K.; Pasbola, K.; Pandey, P.; Sharma, R.; Thakar, A.; Solanki, P.R. Nano-modified screen-printed electrode-based electrochemical immunosensors for oral cancer biomarker detection in undiluted human serum and saliva samples. *Nanoscale Adv.* **2024**, *6*, 705–721. [CrossRef] [PubMed]
51. Ahmadi, M.M.; Jullien, G.A. A wireless-implantable microsystem for continuous blood glucose monitoring. *IEEE Trans. Biomed. Circuits Syst.* **2009**, *3*, 169–180. [CrossRef] [PubMed]
52. Cui, Y.; Kim, H.-S.; Cho, E.S.; Han, D.; Park, J.A.; Park, J.Y.; Nam, W.; Kim, H.J.; Cha, I.-H.; Cha, Y.H. Longitudinal detection of somatic mutations in saliva and plasma for the surveillance of oral squamous cell carcinomas. *PLoS ONE* **2021**, *16*, e0256979. [CrossRef] [PubMed]
53. Romani, C.; Salviato, E.; Paderno, A.; Zanotti, L.; Ravaggi, A.; Deganello, A.; Berretti, G.; Gualtieri, T.; Marchini, S.; D'Incalci, M.; et al. Genome-wide study of salivary miRNAs identifies miR-423-5p as promising diagnostic and prognostic biomarker in oral squamous cell carcinoma. *Theranostics* **2021**, *11*, 2987–2999. [CrossRef] [PubMed]
54. Chen, Z.; Chen, L.; Li, S.; Xia, P.; Lam, A.K.-Y.; Qiao, J.; Liu, Y.; Qiao, B. Integrated analysis of oral rinse-derived and plasma circulating tumour DNA for mutation profiling and outcome prediction with oral squamous cell carcinoma. *npj Precis. Oncol.* **2025**, *9*, 183. [CrossRef] [PubMed]
55. Shpitzer, T.; Bahar, G.; Feinmesser, R.; Nagler, R.M. A comprehensive salivary analysis for oral cancer diagnosis. *J. Cancer Res. Clin. Oncol.* **2007**, *133*, 613–617. [CrossRef] [PubMed]

56. Geiken, A.; Gutman, A.S.; Röder, N.; Holtmann, L.; Graetz, C.; Schwarz, K.; Dörfer, C.E. A new method for continuous in vivo pH measurement in saliva and oral biofilm: A comparative pilot study. *Clin. Oral Investig.* **2026**, *30*, 23. [CrossRef] [PubMed]
57. Lloyd, S.A.; Lee, T.E.; Murphy, E.K.; Doussan, A.F.; Thones, J.P.; Kerr, D.A.; Paydarfar, J.A.; Halter, R.J. In vivo classification of oral lesions using electrical impedance spectroscopy. *IEEE Trans. Biomed. Eng.* **2026**, *73*, 311–321. [CrossRef] [PubMed]
58. Feng, Q.; Bennett, Z.; Grichuk, A.; Pantoja, R.; Huang, T.; Faubert, B.; Huang, G.; Chen, M.; DeBerardinis, R.J.; Sumer, B.D.; et al. Severely polarized extracellular acidity around tumour cells. *Nat. Biomed. Eng.* **2024**, *8*, 787–799. [CrossRef] [PubMed]
59. International Commission on Non-Ionizing Radiation Protection. Guidelines for limiting exposure to electromagnetic fields (100 kHz to 300 GHz). *Health Phys.* **2020**, *118*, 483–524. [CrossRef] [PubMed]
60. Berg, H.C.; Purcell, E.M. Physics of chemoreception. *Biophys. J.* **1977**, *20*, 193–219. [CrossRef] [PubMed]
61. Scharf, L.L.; Friedlander, B. Matched subspace detectors. *IEEE Trans. Signal Process.* **1994**, *42*, 2146–2157. [CrossRef]
62. Page, E.S. Continuous inspection schemes. *Biometrika* **1954**, *41*, 100–115. [CrossRef]
63. Wisniewski, N.; Reichert, M. Methods for reducing biosensor membrane biofouling. *Colloids Surf. B Biointerfaces* **2000**, *18*, 197–219. [CrossRef] [PubMed]
64. Wu, J.; Deng, J.; Theocharidis, G.; Sarrafian, T.L.; Griffiths, L.G.; Bronson, R.T.; Veves, A.; Chen, J.; Yuk, H.; Zhao, X. Adhesive anti-fibrotic interfaces on diverse organs. *Nature* **2024**, *630*, 360–367. [CrossRef] [PubMed]
65. Vickers, A.J.; Elkin, E.B. Decision curve analysis: A novel method for evaluating prediction models. *Med. Decis. Mak.* **2006**, *26*, 565–574. [CrossRef] [PubMed]
66. Karacolak, T.; Hood, A.Z.; Topsakal, E. Design of a dual-band implantable antenna and development of skin mimicking gels for continuous glucose monitoring. *IEEE Trans. Microw. Theory Techn.* **2008**, *56*, 1001–1008. [CrossRef]
67. Liu, X.Y.; Wu, Z.T.; Fan, Y.; Tentzeris, E.M. A miniaturized CSRR loaded wide-beamwidth circularly polarized implantable antenna for subcutaneous real-time glucose monitoring. *IEEE Antennas Wirel. Propag. Lett.* **2017**, *16*, 577–580. [CrossRef]
68. Hassan, R.S.; Lee, J.; Kim, S. A minimally invasive implantable sensor for continuous wireless glucose monitoring based on a passive resonator. *IEEE Antennas Wirel. Propag. Lett.* **2020**, *19*, 124–128. [CrossRef]

Disclaimer/Publisher's Note: The statements, opinions and data contained in all publications are solely those of the individual author(s) and contributor(s) and not of MDPI and/or the editor(s). MDPI and/or the editor(s) disclaim responsibility for any injury to people or property resulting from any ideas, methods, instructions or products referred to in the content.